

Integrating solid direct air capture systems with green hydrogen production: Economic synergy of sector coupling

Sunwoo Kim^{1,2}, Joungho Park³, and Jay H. Lee^{1*}

¹ Mork Family Department of Chemical Engineering and Material Sciences, University of Southern California, 925 Bloom Walk, Los Angeles, CA 90089, USA

² Department of Chemical and Biomolecular Engineering, Korea Advanced Institute of Science and Technology (KAIST), 291, Daehak-ro, Yuseong-gu, Daejeon, 34141, Republic of Korea

³ Energy AI & Computational Science Laboratory, Korea Institute of Energy Research, 71-2 Jang-dong, Yuseong-gu, Daejeon, 305-343, Republic of Korea

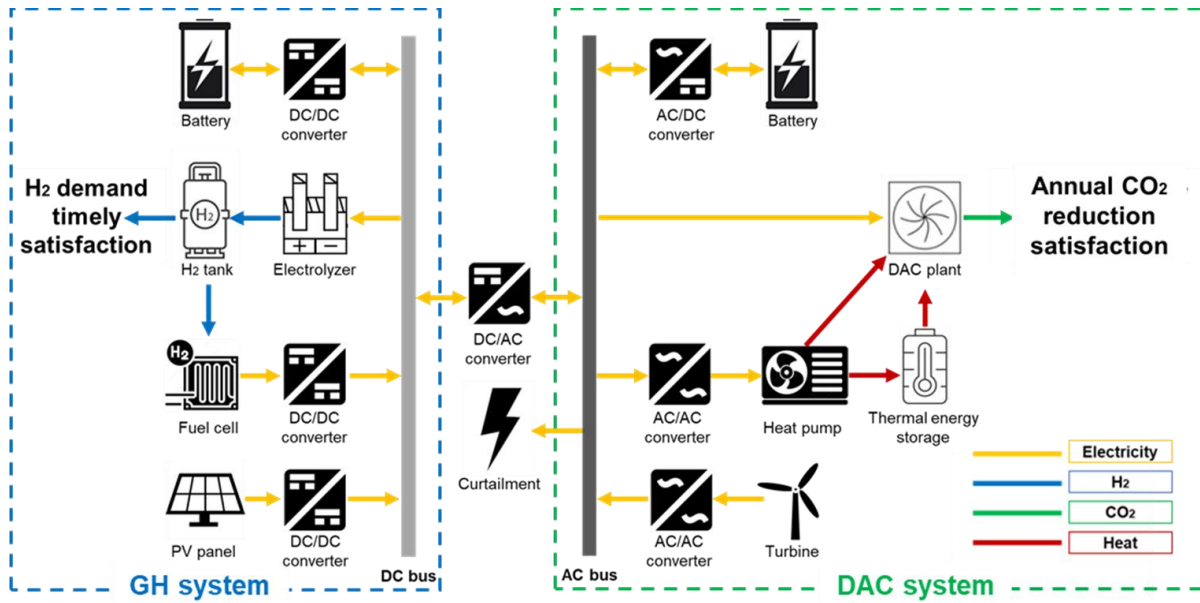
*Corresponding author's E-mail: jlee4140@usc.edu

Abstract

In the global pursuit of sustainable energy solutions, mitigating carbon dioxide (CO₂) emissions stands as a pivotal challenge. With escalating atmospheric CO₂ levels, the imperative of direct air capture (DAC) systems becomes evident. Simultaneously, green hydrogen (GH) emerges as a pivotal medium for renewable energy. Nevertheless, the substantial expenses associated with these technologies impede widespread adoption, primarily due to significant installation costs and underutilized operational advantages when deployed independently. Integration through sector coupling enhances system efficiency and sustainability, while shared power sources and energy storage devices offer additional economic benefits. In this study, we assess the economic viability of polymer electrolyte membrane electrolyzers versus alkaline electrolyzers within the context of sector coupling. Our findings indicate that combining GH production with solid DAC systems yields significant economic advantages, with approximately a 10% improvement for PEM electrolyzers and a 20% enhancement for alkaline electrolyzers. These results highlight a substantial opportunity to improve the efficiency and economic viability of renewable energy and green hydrogen initiatives, thereby facilitating the broader adoption of cleaner technologies.

Keywords: Solid direct air capture, Green hydrogen, Alkaline and PEM electrolyzer, Sector coupling

Graphical abstract



Benefit of sector coupling

- Enhanced economic viability of hydrogen production and direct air capture costs
- Stronger synergy effect for alkaline electrolyzers compared to PEM electrolyzers

Main

The imperative for a sustainable global society increasingly focuses on mitigating anthropogenic carbon dioxide (CO₂) emissions.[1-3] Direct air capture (DAC) systems are gaining recognition as a vital technology for recovering atmospheric CO₂. [4-6] This perspective is supported by a growing consensus among research entities and governments that a transition to clean, renewable energy must be complemented by technologies capable of actively extracting CO₂ from the atmosphere.[7, 8]

Among the diverse technologies in DAC, temperature-vacuum swing adsorption (TVSA) with solid adsorbents is emerging as a particularly promising method.[9, 10] Solid DAC systems offer better energy efficiency compared to their liquid counterparts and demonstrate significant operational flexibility, which is crucial for adapting to the variability of energy sources, particularly those based on renewables.[11] Solid DAC systems operate in two phases: adsorption and desorption.[12] During adsorption, CO₂ is captured from the atmosphere using solid adsorbents. In the desorption phase, the captured CO₂ is released for storage. This process is more energy-efficient than liquid DAC, leading to lower operational costs.[13] Additionally, the ability of solid DAC systems to enter a shutdown state provides unmatched adaptability to fluctuating renewable energy availability.[14] However, the high installation costs of solid DAC facilities necessitate operating at high loads to achieve economic viability in the standalone solid DAC system.

In tandem with DAC, the role of green hydrogen (GH) as a sustainable energy carrier is becoming increasingly significant.[15-19] GH refers to hydrogen produced by utilizing renewable energy sources, typically through methods like water electrolysis, including those employing Proton Exchange Membrane (PEM) and alkaline electrolyzers.[20-22] However, the intrinsic variability of renewable energy sources, coupled with the requirement for timely satisfaction of hydrogen demand, can lead to oversized GH facilities and energy wastage through curtailment.[23, 24] Consequently, the operational flexibility advantages inherent in both technologies are not fully realized when deployed as standalone systems. Therefore, adopting a sector coupling strategy presents a promising avenue to improve economic feasibility and efficiency in this domain.

Our study scrutinizes the integration of solid DAC systems with GH system through sector coupling to address existing challenges. To efficiently integrate this variable energy, a coupling of the power sector to the residential, transport, industry, and commercial/trade sector is often promoted, which is called sector coupling.[25] This approach ensures an optimal alignment of energy supply and demand when paired with GH production, leveraging the strengths of both technologies to enhance overall system efficiency and sustainability. Additionally, sharing power sources and energy storage devices can offer further economic benefits to the sector-coupled system.

The concept of sector coupling has been acknowledged for its potential to synergistically integrate renewable energy systems, offering economic and energy efficiency benefits [26, 27]. Rafael et al. explored the potential of sector coupling in carbon capture and storage (CCS) within industrial settings such as cement production, steel manufacture, and waste incineration.[28] By sector coupling, significant emission reductions of up to 860 Mt of

CO₂ annually in Europe alone, equivalent to nearly 27% of European GHG emissions, are estimated. Furthermore, the integrated approach yields notable economic benefits, with cost savings of approximately 50% compared to standalone CCS technologies, emphasizing the importance of system integration in achieving net-zero and net-negative industrial sectors. Another study delved into the integration of renewable energy across Europe using the PyPSA-Eur-Sec-30 model, concentrating on the implications of sector coupling and the expansion of cross-border transmission networks.[29] Their research emphasizes the pivotal role of technologies such as battery electric vehicles, power-to-gas units, and long-term thermal energy storage in realizing a 95% decrease in CO₂ emissions by 2050. Further research supports using hydrogen for long-duration energy storage in grids dependent on variable renewable energy, advocating an integrated approach for electricity and hydrogen supply chains.[30] Favoring power-to-hydrogen pathways over power-to-gas-to-power strategies could enhance renewable energy utilization and decrease overall system costs, particularly in scenarios targeting extensive decarbonization.

Despite the growing interest in sector coupling as a means to boost renewable energy efficiencies, there's a notable lack of research exploring the advantages of linking GH with solid DAC systems. Furthermore, there is lack of research that comparatively evaluate the economic feasibility of polymer electrolyte membrane (PEM) electrolyzer and Alkaline electrolyzer under sector coupling. The minimum operating threshold for GH production varies depending on the type of water electrolyzer. PEM electrolyzers have a lower minimum operating threshold due to their use of a solid polymer electrolyte, which allows efficient proton conduction and rapid response to varying electrical inputs. In contrast, alkaline electrolyzers require a higher minimum current to maintain effective electrochemical reactions because they use a liquid electrolyte, typically potassium hydroxide, necessitating more stable operating conditions. These differing characteristics of electrolyzers result in varying degrees of synergy with solid DAC in sector-coupling applications. We investigate the synergistic behavior of each electrolyzer technology by varying the ratio between hydrogen demand and CO₂ removal targets, as well as how the installation costs of these facilities influence the economic viability of each system and their synergy variations. This gap highlights a compelling opportunity to not only enhance the efficiency and economic feasibility of renewable energy and green hydrogen initiatives but also to advance the development and adoption of DAC technologies.

System description

In this research, we examine five distinct scenarios: one featuring a GH system and a solid DAC system, both powered by renewable energy, alongside three configurations of systems where these technologies are integrated through sector coupling. In each scenario, wind turbines[31] and photovoltaic (PV) panels[32, 33] generate electricity from wind and solar energy, respectively. Energy storage is facilitated through batteries[34], hydrogen tanks (HT)[35], and thermal energy storage (TES)[14], storing electricity, hydrogen, and thermal energy, correspondingly. Water electrolysis[36, 37], performed by electrolyzers, splits water into oxygen and hydrogen gases, while fuel cells[38] convert hydrogen back into electricity.

Heat pumps are utilized to transform electricity into thermal energy.[14, 39] Curtailment refers to the process of dissipating energy or idling turbines to prevent grid overload.

Given the differing current types required by each facility, efficient energy integration and operation necessitate suitable converters and bus configurations. Electrolyzers and batteries operate on direct current (DC), whereas heat pumps and DAC plants require alternating current (AC). We assume converter efficiencies of 98% for both DC/DC and AC/AC, and 95% for AC/DC conversions in our analysis.[40]

In Fig. 1 (a), the focus of the GH system is on meeting hydrogen demand promptly, with the primary energy consumption directed towards powering the water electrolyzer. Consequently, it is most efficient to configure the water electrolyzer to operate on a DC bus. Excess energy is stored as electricity in batteries and as hydrogen in HT. Additionally, any surplus hydrogen may be converted back into electricity using a fuel cell, ensuring that the system meets the minimum operational requirements of the water electrolysis process.[41] This will be explained further in the Supplementary Materials.

In Fig. 1 (b), the solid DAC system is designed with a goal of achieving an annual average CO₂ capture target, making energy supply to the DAC plant its principal energy demand. As such, configuring the DAC plant to utilize an AC bus is the most efficient approach. Excess energy is stored in the form of electricity in batteries and as thermal energy in TES systems. Additionally, the system includes a heat pump, which is subject to a minimum operational requirement.[42] This will be explained further in the Supplementary Materials.

Fig. 1 (c) depicts the integration of GH and solid DAC systems within a sector-coupled framework. Fig. 1 (c) presents a hybrid DC-AC system, a purely DC setup and an AC setup can be found in the Supplementary Material, Fig. B. 1 and Fig. B. 2, respectively. Across all configurations, the systems are designed to ensure prompt satisfaction of hydrogen demand and to meet an annual average target for CO₂ removal. Each configuration employs a unique arrangement of facilities and converters to match its electrical current requirements. Specifically, the DC setup is optimized for GH efficiency but performs less efficiently for the DAC plant. Conversely, the AC setup offers high efficiency for the DAC plant at the expense of GH efficiency. The hybrid DC-AC configuration achieves high efficiency within each respective bus but faces challenges with power exchange efficiency between DC and AC buses. This necessitates a thorough analysis to determine the most effective configuration for achieving the objectives of the sector-coupled system. This will be explained further in the Supplementary Materials.

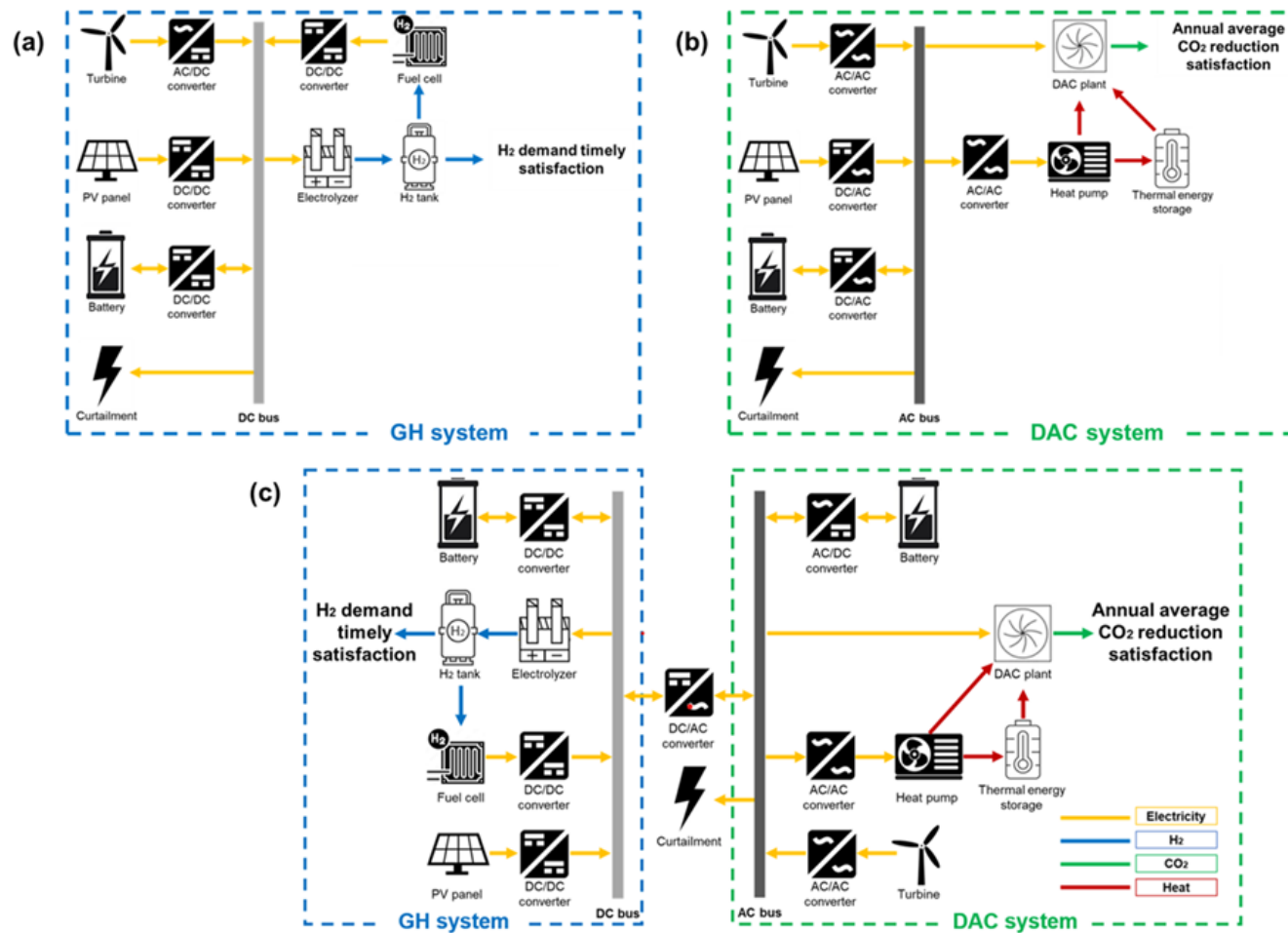


Fig. 1. (a) The Green Hydrogen (GH) system operating in a Direct Current (DC) configuration, designed to ensure the timely fulfillment of hydrogen demand, (b) Renewable-based Solid DAC System: Operating under an Alternating Current (AC) configuration, aimed at achieving an CO₂ reduction target on an annual average basis throughout the project's duration, (c) Integrated sector coupling system of GH and solid DAC, configured to operate between DC and AC, to balance the objectives of timely satisfaction of hydrogen demand and achieving annual CO₂ reduction targets over the project's duration.

Evaluation metrics

The economic performance of the system is assessed using two primary metrics: the Levelized Cost of producing Hydrogen (LCOH) and the Levelized Cost of DAC (LCOD), defined by equation (2) and equation (3), respectively.

$$LCOH = \frac{TAC^{GH}}{\text{Annual GH production}} = \frac{TAC^{GH}}{\frac{1}{N^{sc}} \times \sum_{sc} \sum_t \left[p2h_{sc,t} \times \frac{1}{\eta^W} \right]} \quad (2)$$

$$LCOD = \frac{TAC^{DAC}}{\text{Annual CO}_2 \text{ reduction}} = \frac{TAC^{DAC}}{\frac{1}{N^{sc}} \times \sum_{sc} \sum_t [dac_{sc,t}^3]} \quad (3)$$

In the above, TAC^{GH} denotes the total annualized cost (TAC) of the standalone GH system and TAC^{DAC} corresponds to the TAC of standalone solid DAC system, respectively. N^{sc} denotes the number of scenarios, $p2h_{sc,t}$ presents the power rate to the electrolyzer for scenario sc at time t , η^W indicates the conversion efficiency of the electrolyzer, and $dac_{sc,t}^3$ denotes the desorption CO_2 flow rate of solid DAC plant for scenario sc at time t .

For evaluating the economic synergy of sector coupling, we define two metrics. The metric termed *Improvement* represents the difference in Total Annualized Cost (TAC) between the combined system and the sum of the standalone systems. Additionally, there exists another metric referred to as *Synergy* which denotes the ratio of the TAC difference to the sum of the standalone TAC, while ensuring timely hydrogen supply and achieving the annual CO_2 reduction target. The economic metrics are expressed as follows:

$$\text{Improvement (MM\$/yr)} = TAC^{GH} + TAC^{DAC} - TAC^{Combined} \quad (4)$$

$$\text{Synergy (\%)} = 1 - \frac{TAC^{Combined}}{TAC^{GH} + TAC^{DAC}} \quad (5)$$

In the above, $TAC^{Combined}$ indicates the TAC of the sector-coupled system. A Synergy value of 0 signifies no economic advantage from the coupling, whereas a higher Synergy value indicates increasing economic benefits.

Techno-economic analysis of standalone GH and DAC system

We conducted an economic evaluation of standalone GH and DAC systems across different regions. We chose three locations—Antofagasta, Bundaberg, and Neom—each offering promising renewable energy potential and distinct meteorological profiles. To accommodate the unpredictability of renewable energy sources, we identified and economically appraised the optimal design under three annual scenarios for solar and wind.

The specifics of this optimization process and detailed problem description are outlined in the Supplementary Materials.

In Fig. 2 (a), the LCOH for PEM electrolyzers ranges from \$3.2/kg H₂ to \$3.6/kg H₂. The primary cost component is attributed to power sources, encompassing turbines and PV panels, followed by electrolyzers and energy storage devices. Conversely, in Fig. 2 (b), LCOH values for alkaline electrolyzers range from \$3.7/kg H₂ to \$4.3/kg H₂, approximately 15% higher than PEM electrolyzers. The increased minimum operating threshold of alkaline electrolyzers escalates battery costs, alongside similar impacts on power sources and fuel cells. However, the installation cost advantage of alkaline electrolyzers reduces the electrolyzer cost element compared to PEM counterparts. Fig. 2 (c) depicts the LCOD in various regions, ranging from \$80/t CO₂ to \$86/t CO₂, with DAC facilities as the largest cost driver, trailed by batteries and power sources. The high capital expenditure associated with solid DAC facilities necessitates operating at ~90% load to achieve economic viability in a standalone solid DAC system.

Moreover, we conducted sensitivity analyses, varying facility costs by $\pm 20\%$. In Fig. 3 (a), changes in power sources, electrolyzers, and battery costs exhibit the greatest impact on LCOH for PEM electrolyzer GH systems, whereas Fig. 3 (b) demonstrates a different order of influence which is power sources, battery, and electrolyzer. Fig. 3 (c) reveals that DAC, power sources, and battery costs primarily affect LCOD. Significantly, enhanced operating flexibility of heat pumps markedly reduces LCOD, as depicted in Fig. 4 (d). A 10% reduction in the minimum load threshold corresponds to a ~4% LCOD reduction, equating to approximately \$3/t CO₂, despite facility costs remaining constant. This underscores the surprising capacity of heat pump flexibility to substantially lower overall costs.

Conclusively, our analysis examines how variations in power sources, battery, electrolyzer, and DAC facilities' cost impact on the economic feasibility and synergies of sector-coupled systems as well as the operating flexibility of heat pump.

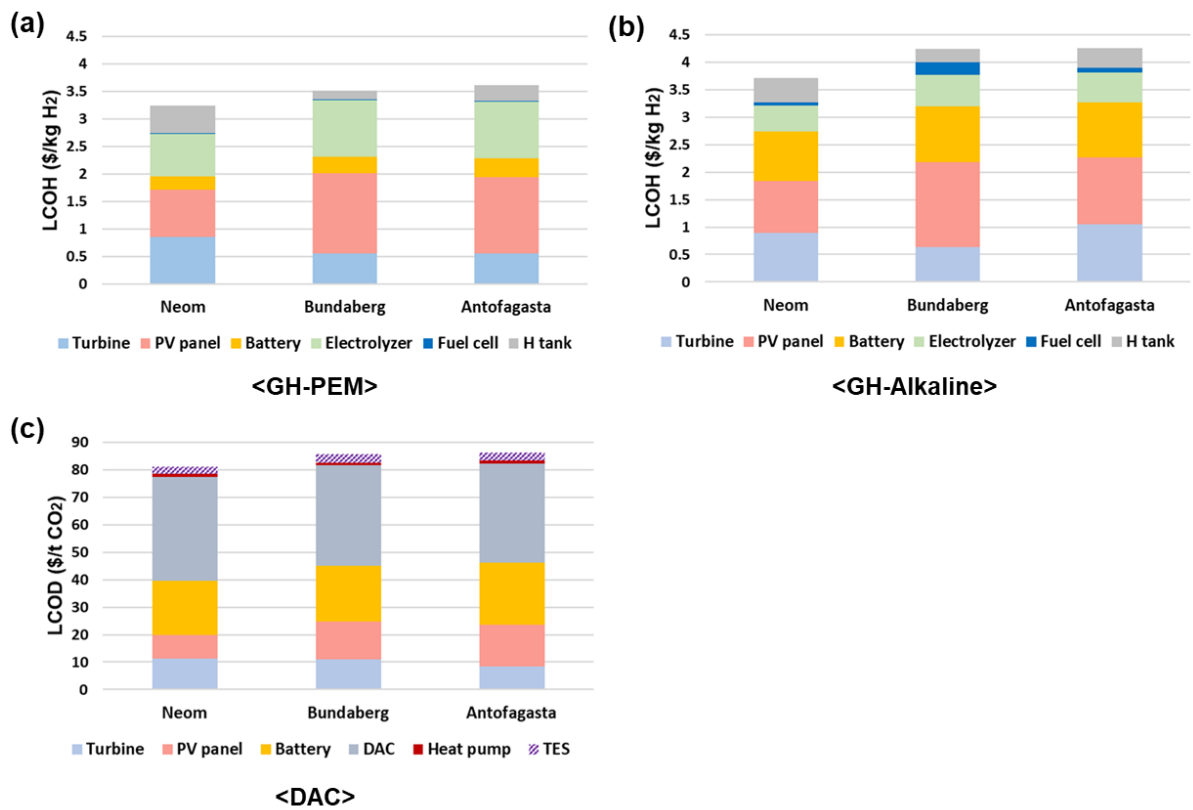


Fig. 2. Cost breakdown of standalone green hydrogen system and DAC system by varying regions: (a) PEM electrolyzer-based standalone green hydrogen system, (b) Alkaline electrolyzer-based standalone green hydrogen system, (c) standalone solid DAC system. The light-blue bar indicates turbine, apricot bar represents PV panel, orange bar denotes battery, green bar indicates electrolyzer, blue bar indicates fuel cell, grey bar denotes hydrogen tank, dark blue bar represents solid DAC facility, red bar indicates heat pump, and purple patterned bar denotes the thermal energy storage devices.

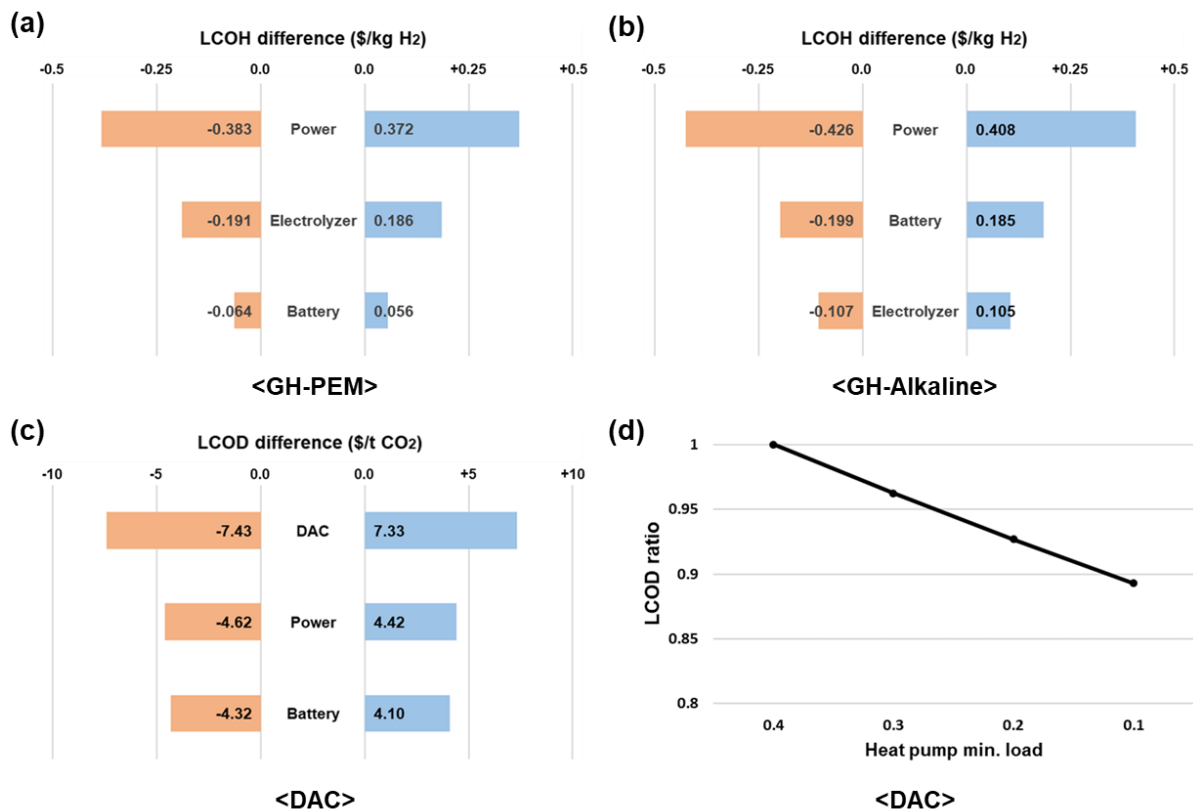


Fig. 3. (a) Sensitivity analysis of cost variations ($\pm 20\%$) for different components in standalone green hydrogen and DAC systems. (a) PEM electrolyzer-based green hydrogen system, (b) Alkaline electrolyzer-based green hydrogen system, (c) Solid DAC system, and (d) Minimum load of heat pumps in a standalone solid DAC system. The blue bar indicates $+20\%$ cost increased cases and red bars represents -20% cost reduction cases for each facility.

Economic evaluation and synergy assessment of sector-coupled system

Our study evaluates the economic advantages of a sector-coupled system integrating solid DAC with GH production, compared against the standalone solid DAC and GH systems. In the defined baseline scenario, the GH system is designed to fulfill a constant timely hydrogen demand of 10 kt every year, which is the general capacities of existing steam methane reforming plant. For the solid DAC system, we assess the combined economic impact of sector coupling across a range of average annual CO₂ removal rate, from 0.1 Mt to 1.3 Mt with 0.2 Mt increments. In terms of molar quantities, approximately 0.2 Mt of CO₂ corresponds to the 10 kt of hydrogen.

During our previous session, we observed that the PEM electrolyzer demonstrated approximately 15% greater cost-effectiveness compared to its alkaline counterpart. However, within a sector-coupled framework, the alkaline electrolyzer exhibited a slight advantage, being about 2% more economically efficient than the PEM variant. In the context of a standalone green hydrogen system, a substantial disparity in economic viability existed between the two

electrolyzer types. Nevertheless, when integrated within a sector-coupled system, this gap diminished notably, with the alkaline electrolyzer even surpassing the PEM variant in economic feasibility.

In Fig. 4, alkaline electrolyzer-based system shows an ~1.7 MM\$ decrease in TAC, attributed to their lower cost, albeit requiring ~0.5 MM\$ more in PV panel installations compared to PEM electrolyzer-based system. Notably, in the standalone green hydrogen system, the alkaline electrolyzer demanded three times larger batteries and power sources than the PEM electrolyzer due to a high minimum load of 20%. However, within the sector-coupled paradigm, the economic advantages of shared infrastructure, particularly batteries and power sources with the DAC system, became significant.

Fig. 5 (a) underscores the synergy between 2-11 MM\$ when PEM electrolyzers and DAC are sector-coupled, with this synergy increasing steadily as the CO₂ removal rate rises. At an annual hydrogen production of 10 kt, the highest percentage synergy occurs when the CO₂ removal rate ranges between 0.3-0.5 Mt/yr.

Conversely, Fig. 5 (b) illustrates that the synergy within the sector-coupled scenario of alkaline electrolyzers and DAC ranges between 7-18 MM\$, with a similar trend of increasing synergy as CO₂ removal rate rises. However, the highest percentage synergy is observed when the CO₂ removal rate is at 0.1 Mt/yr, gradually decreasing as the removal rate increases.

The rationale behind the greater synergy observed with alkaline electrolyzers lies in the costly nature of DAC installations, necessitating the optimal design of deploying numerous batteries operating at a high average rate. Through sector coupling, the shared utilization of facilities minimizes the need for excessive battery investment, mitigating the operational inflexibility associated with alkaline electrolyzers. Consequently, despite their intrinsic operational limitations, the cost advantage of alkaline electrolyzers over PEM variants becomes more pronounced within this integrated framework.

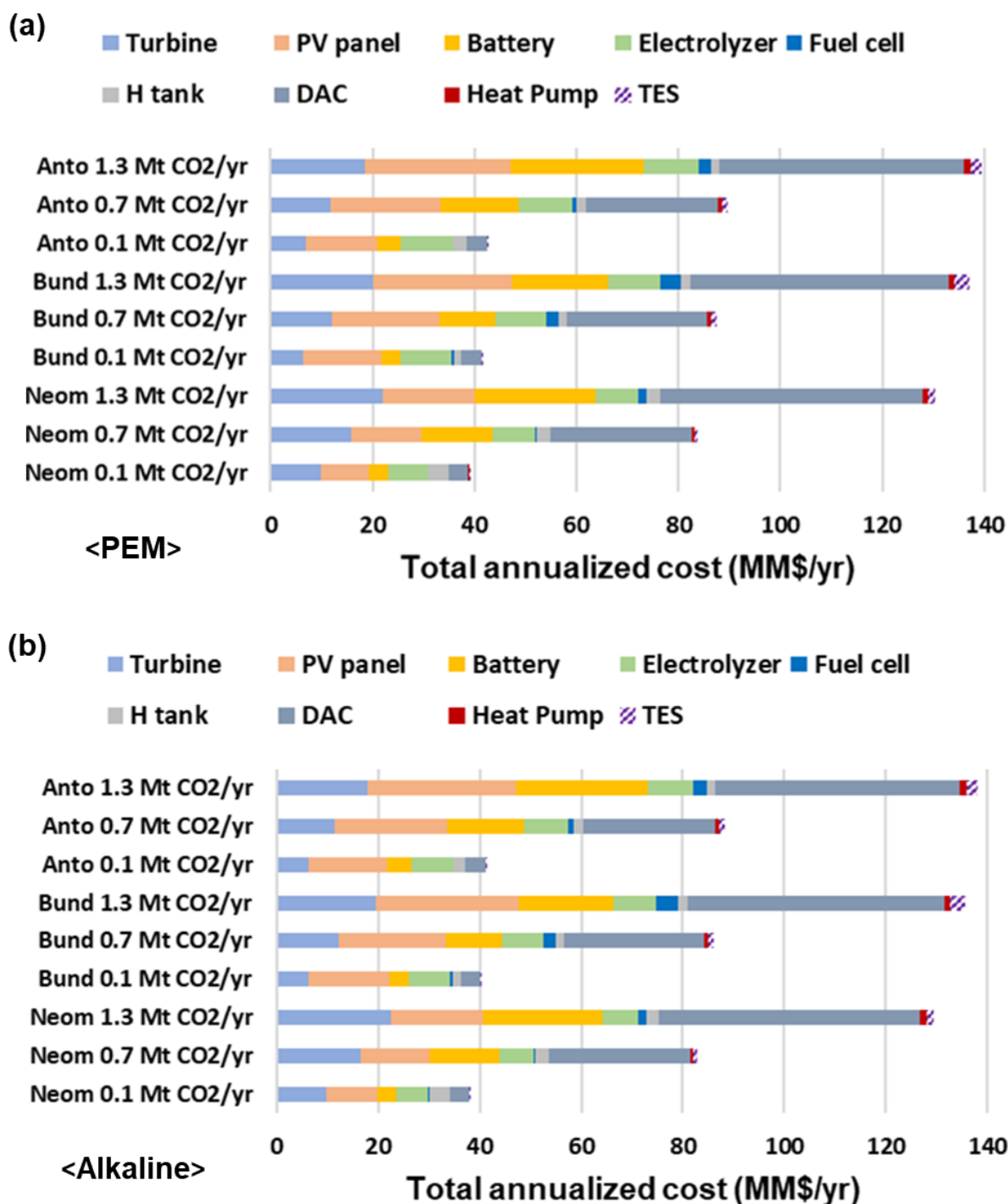


Fig. 4. TAC breakdown of sector-coupled systems across different regions and CO₂ removal rates: (a) PEM electrolyzer-based sector-coupled system, (b) Alkaline electrolyzer-based sector-coupled system. The light-blue bar indicates turbine, red bar represents PV panel, orange bar denotes battery, green bar indicates electrolyzer, blue bar indicates fuel cell, grey bar denotes hydrogen tank, dark blue bar represents solid DAC facility, dark red bar indicates heat pump, and purple pattern denotes the thermal energy storage devices.

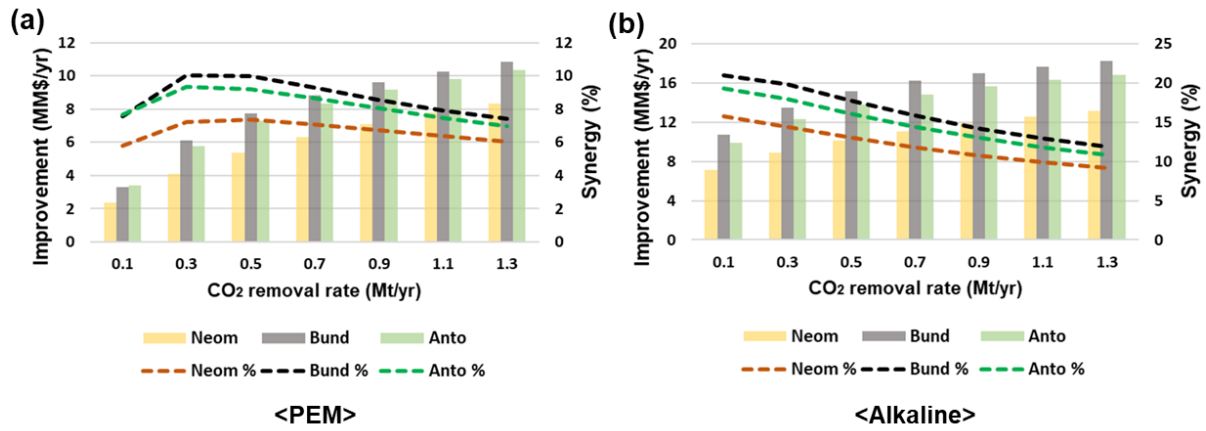


Fig. 5. Improvement (MM\$/yr) and synergy (%) of sector-coupled system across different regions by varying CO₂ removal rate: (a) PEM electrolyzer-based sector-coupled system, (b) Alkaline electrolyzer-based sector-coupled system. The yellow bar indicates improvement at Neom, the grey bar denotes improvement at Bundaberg, and the green bar represents improvement at Antofagasta. The red dashed line denotes synergy at Neom, the black dashed line represents synergy at Bundaberg, and the green dashed line indicates synergy at Antofagasta.

Techno-economic analysis of sector-coupled system and their synergy variation

We examine how variations in facility costs impact the economic feasibility and synergies of sector-coupled systems, critical given uncertainties in future renewable technology cost projections. This endeavor aims to illuminate the potential synergies within sector-coupled systems across diverse future scenarios. Consequently, it becomes imperative to scrutinize the economic implications and synergistic effects within our proposed sector coupling model when there are substantial fluctuations in the costs of key facilities. This session focuses on assessing the variations in synergy and TAC when the costs of individual facilities escalate by 20% from the baseline scenario. The evaluation criteria comprise TAC difference (MM\$/yr) and synergy difference (%). Specifically, we analyze the impacts of a 20% cost increase for each of the following facilities: battery, DAC, electrolyzer, and power source.

In Fig. 6 (a), a noticeable trend emerges where the TAC difference escalates with increasing CO₂ removal rates in the sector-coupled system employing PEM electrolyzer. Specifically, a 20% surge in the power source price results in a TAC increment of approximately 4 MM\$/yr at a CO₂ removal rate of 0.1 Mt/yr, and this figure rises to about 9 MM\$/yr at a CO₂ removal rate of 1.3 Mt/yr. Similarly, a 20% hike in DAC facility costs leads to a TAC rise of around 1 MM\$/yr at a CO₂ removal rate of 0.1 Mt/yr, while this figure elevates to about 10 MM\$/yr at a CO₂ removal rate of 1.3 Mt/yr. Likewise, a 20% increase in battery

costs results in a TAC increase of approximately 0.8 MM\$/yr at a CO₂ removal rate of 0.1 Mt/yr, which jumps to about 4.3 MM\$/yr at a CO₂ removal rate of 1.3 Mt/yr. Notably, a 20% rise in electrolyzer costs leads to a consistent TAC increase of about 2 MM\$/yr across all CO₂ removal rates.

However, when considering synergy difference, a clear contrast emerges between the two systems. Fig. 6 (c) illustrates that when battery costs are heightened compared to the base case, the synergy difference escalates from +0.35% to +0.8% with a 20% increase in battery costs, primarily due to the augmented CO₂ removal rate. Conversely, Fig. 6(d) showcases a decrease in synergy difference from 2.1% to 1.35% as CO₂ removal rates increase. This discrepancy arises from the fact that the TAC of the standalone Alkaline GH system is approximately three times more sensitive to battery costs than the PEM electrolyzer, as evidenced in Fig. 3. Moreover, Figs. 6 (a) and (b) depict that as battery costs in the sector-coupled system rise, the TAC difference increases nearly proportionally with the CO₂ removal rate. Essentially, the sector-coupled system employing an alkaline electrolyzer demonstrates a more substantial synergy difference compared to the system with a PEM electrolyzer. Additionally, as CO₂ removal rates escalate, the proportion of TAC of the standalone GH system in the denominator of Synergy diminishes, indicating an inverse trend.

Regarding a 20% increase in DAC facility costs, both systems exhibit a similar trajectory, with a synergy difference of approximately -0.3% at a CO₂ removal rate of 0.1 Mt/yr and about -0.6% at 0.5-1.3 Mt/yr. Typically, high installation costs for DAC units necessitate opting for smaller capacities operating at higher average rates to maintain cost-effectiveness. Consequently, as DAC unit installation costs decrease, the benefits of sector coupling become more apparent. Reduced installation costs encourage the expansion of DAC's optimal capacity, facilitating more dynamic DAC system operation.

When examining electrolyzers, akin to DACs, the advantages of sector coupling diminish as electrolyzer costs rise, leading to smaller installations and higher average operating rates. Moreover, as the CO₂ removal rate escalates, the impact of increased electrolyzer costs on synergy difference decreases due to the reduced contribution of the standalone GH system to the sector-coupled system's TAC. However, there exists a disparity in magnitude between the two systems: in the sector-coupled system employing PEM electrolyzer, the synergy difference stands at -0.2% at a CO₂ removal rate of 0.1 Mt/yr and -0.1% at 1.3 Mt/yr. Conversely, in the system utilizing an alkaline electrolyzer, the synergy difference is -1.25% at 0.1 Mt/yr and -0.4% at 1.3 Mt/yr. Notably, the PEM electrolyzer in the standalone GH system exhibits approximately twice the sensitivity to electrolyzer costs compared to the alkaline electrolyzer.

In a sector-coupled setup, a 20% increase in electrolyzer costs results in a TAC hike of 2 MM\$/yr for PEM electrolyzers and 1.5 MM\$/yr for alkaline electrolyzers, irrespective of the CO₂ removal rate. This implies that in the sector-coupled system employing PEM electrolyzers, the denominator TAC in the synergy difference experiences a more pronounced increase due to the rise in electrolyzer costs compared to the numerator, in contrast to the system with alkaline electrolyzers. Consequently, the synergy difference is smaller in the PEM electrolyzer system compared to the alkaline electrolyzer system.

An intriguing finding emerges when the cost of the power source facility (turbine, PV panel) is increased by 20%. In the system utilizing PEM electrolyzer, a negative synergy difference is observed when the CO₂ removal rate is below 0.5 Mt/yr, but a positive synergy difference emerges beyond that threshold. To elucidate this, it's crucial to recognize that the power source facility serves dual roles in terms of sector coupling synergy. Firstly, it supplies variable electricity necessary for the dynamic operation of DAC and electrolyzer systems. Essentially, more renewable energy supply is required to enable the dynamic operation of these systems, thereby enhancing sector coupling synergy. Secondly, the power source facility facilitates cost reduction by preventing over-sizing through shared facilities like batteries.

Consequently, as costs escalate, synergy difference increases akin to batteries. Therefore, in both systems, as CO₂ removal rates rise, synergy difference escalates due to the relatively larger impact of the second factor compared to the first.

Interestingly, in both systems, at each CO₂ removal rate, the sum of synergy differences for a 20% increase in the installed price of a major facility nearly equals zero. Thus, irrespective of overarching technological advancements or regressions, the synergistic effects exhibit a notable constancy when juxtaposed with those discerned in the foundational scenario. In essence, the advantages conferred by sector coupling endure notwithstanding the evolution of renewable energy technology.

The economic benefits of sector coupling are notably influenced by easing the minimum operational constraints of the heat pump, which serves the DAC unit by converting electricity into heat. In the baseline scenario, the large-scale heat pump's minimum operational threshold is set at 0.4[42], with subsequent analyses exploring the effects of reducing this threshold to 0.1 overcoming scale-up issues.[14, 39] Examining Figs. 7 (a) and (b), it's evident that the TAC decreases as the minimum load of the heat pump diminishes, thereby enhancing operating flexibility. The TAC ratio, defined as the ratio of TAC when the minimum load of the heat pump is reduced to that when it's set at 40% (the base case), reflects this trend. A smaller TAC ratio indicates a greater reduction in TAC compared to the base case. In both systems, as the CO₂ removal rate rises, the reduction in TAC ratio intensifies with decreasing minimum load of the heat pump. For instance, at a CO₂ removal rate of 0.1 Mt/yr, a 10% increase in the operating flexibility of the heat pump leads to approximately a 1% decrease in the TAC ratio. This reduction increases to about 2.7% at a CO₂ removal rate of 1.3 Mt/yr.

Turning to Figs. 7 (c) and (d), the overall Synergy trend in the base case remains consistent, albeit with slight variations. Specifically, in the sector-coupled system employing PEM electrolyzer, synergy increases by up to 1% when the CO₂ removal rate is below 0.9 Mt/yr due to enhanced operating flexibility of the heat pump. Conversely, for CO₂ removal rates exceeding 1.1 Mt/yr, synergy experiences a minor decline as the operating flexibility of the heat pump increases. Conversely, in the system with an alkaline electrolyzer, while the overall trend aligns, synergy attributed to the operating flexibility of the heat pump gradually diminishes as the CO₂ removal rate rises. This phenomenon arises from the fact that as heat pump flexibility increases, the synergy decreases due to improved economics of the standalone DAC system. This observation emphasizes the symbiotic dynamics within the components of the sector-coupled system and highlights the critical need for system-wide optimization to fully leverage the collective advantages.

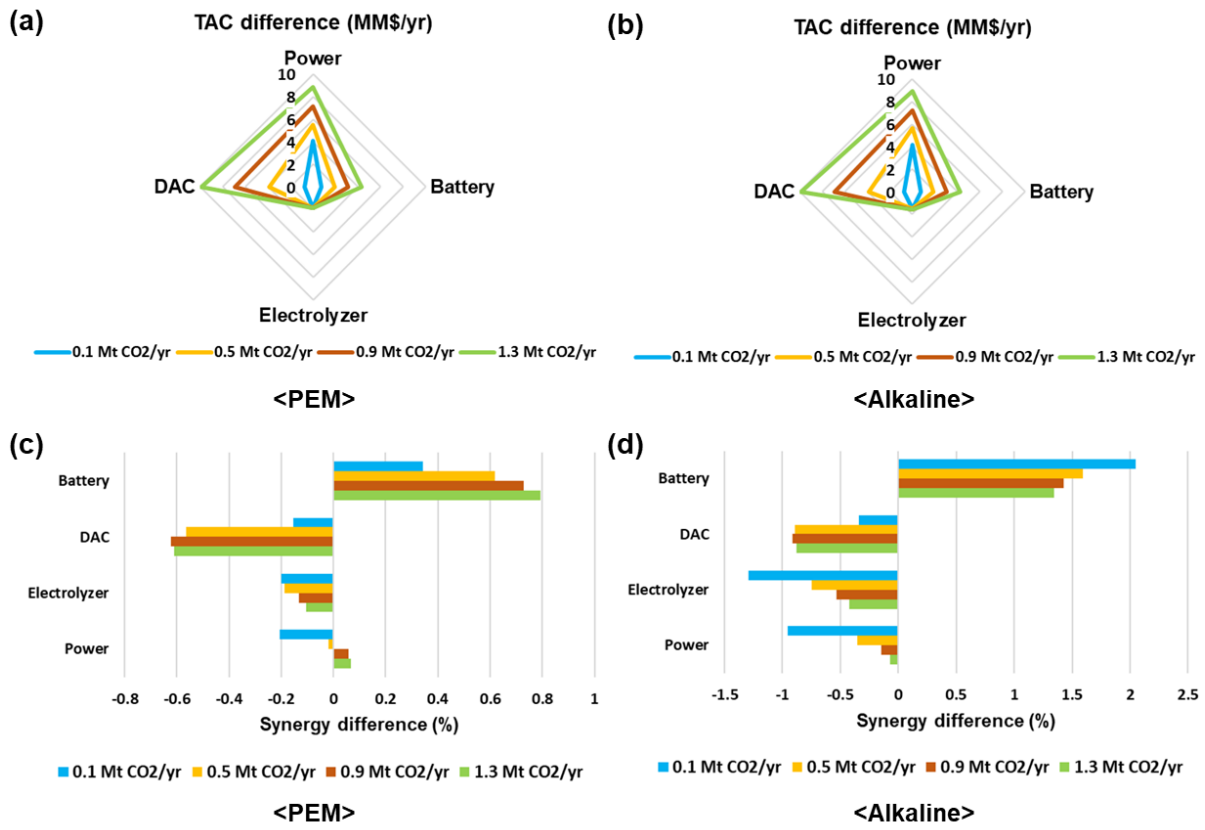


Fig. 6. TAC difference (MM\$/yr) variation resulting from a 20% increased cost in the cost of each facility while varying CO₂ removal rate in the sector-coupled system: (a) PEM electrolyzer-based sector-coupled system, (b) Alkaline electrolyzer-based sector-coupled system, Synergy difference (%) variation resulting from a 20% increase in the cost of each facility while varying the CO₂ removal rate in the sector-coupled system: (c) PEM electrolyzer-based sector-coupled system, (d) Alkaline electrolyzer-based sector-coupled system (light-blue color indicates 0.1 Mt CO₂/yr case, yellow color represents 0.5 Mt CO₂/yr case, brown color denotes 0.9 Mt CO₂/yr case, and light-green color indicates 1.3 Mt CO₂/yr).

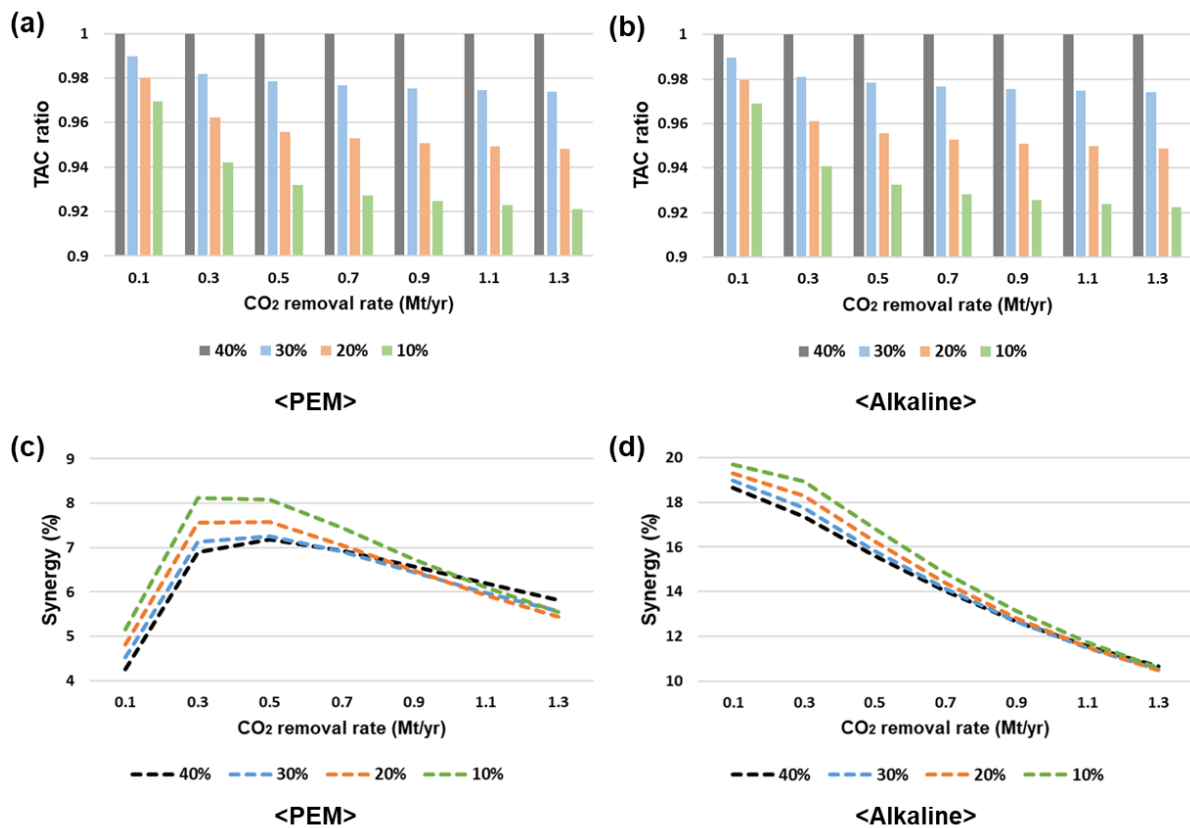


Fig. 7. TAC ratio referenced in the base case across different heat pump minimum loads by varying CO₂ removal rate for (a) PEM electrolyzer-based sector-coupled system and (b) Alkaline electrolyzer-based sector-coupled system. Synergy (%) across different heat pump minimum loads by varying CO₂ removal rate for (c) PEM electrolyzer-based sector-coupled system and (d) Alkaline electrolyzer-based sector-coupled system (black color indicates the base case, blue represents 30% minimum load of the heat pump case, red denotes 20% minimum load of the heat pump case, and green represents 10% minimum load of the heat pump case).

Conclusion

This study presents an extensive optimization-based approach for integrating solid Direct Air Capture (DAC) systems with Green Hydrogen (GH) production, aimed at addressing the dual challenges of reducing anthropogenic CO₂ emissions and enhancing the efficiency of renewable energy usage. We concentrated on evaluating the economic benefits of sector coupling within three distinct regions—Antofagasta, Bundaberg, and Neom—each characterized by unique renewable energy capacities and meteorological conditions.

The key findings derived from our analysis are as follows:

- The combination of GH production with solid DAC systems delivers significant economic benefits: ~10% for PEM electrolyzer, ~20% for alkaline electrolyzer.
- Alkaline electrolyzer superior PEM electrolyzer in the sector-coupled system although the economic feasibility of standalone GH system was ~15% lower.
- Economic advantages derived from sector coupling are significantly affected by the specific ratio of annual hydrogen production to the system's average annual CO₂ reduction goal.
- The cost-effectiveness of sector coupling is enhanced by increased battery cost, decreased DAC facility and electrolyzer cost, and impact of power sources cost depends on CO₂ removal targets.
- The robustness of sector coupling in enhancing efficiency and sustainability is underscored by its enduring benefits, which remain significant irrespective of future developments in renewable energy technology.
- Increased flexibility in operating constraints for heat pumps boosts the economic viability of sector coupling, particularly for lower CO₂ removal targets.

In summary, our study proposes the sector coupling strategy of integrating GH production with solid DAC systems, and offers valuable insights into its economic advantages, contributing to the broader discourse on sustainable energy solutions. Sector coupling gives more opportunity to alkaline electrolyzer compared to PEM electrolyzer. These findings serve as a resource for policymakers, industry stakeholders, and researchers committed to advancing a low-carbon future.

Methods

The Two-stage Stochastic Programming (2SSP) approach is utilized to determine the optimal system capacity and operational strategies that effectively manage uncertainties.[43, 44] This methodology requires decision-makers to make two sequential sets of decisions. The first-stage decisions dictate the capacity of the various facilities, while the second-stage

decisions revolve around managing the energy system under uncertainties such as wind speed variability, solar Global Horizontal Irradiance (GHI). Initially, first-stage decisions are made with an incomplete knowledge of future uncertainties, focusing on system design choices such as capacity and infrastructure investments. Subsequently, second-stage operational decisions are made in response to the actual realization of weather scenarios, based on the infrastructure established in the first stage. These decisions are aimed at optimizing capacity investment and resilient energy management to real-world conditions.

The goal of our model is to minimize the total annualized cost (TAC), encompassing the expenses related to installation, operation, and maintenance as below:

$$\min TAC = \sum_i \left[IC^i \times X_i \times (CRF^i + OM^i) \right] \quad \text{where} \quad CRF^i = \frac{r \times (1+r)^L}{(1+r)^L - 1} \quad (1)$$

In above equation, for facility i , IC^i stands for its investment cost, X_i denotes the capacity, CRF^i signifies the capital recovery factor, and OM^i represents the operating and maintenance cost, assumed to be proportional to the installation cost. The economic parameters of facilities are summarized in below Table 1.

Equation (1) outlines the objective function, with constraints defined by energy balance equations and mathematical models of the facilities detailed in the Supplementary Materials, equation (A1-28). For example, the constraints for the standalone GH system are specified in equation (A1-12), whereas the standalone DAC system is governed by equation (A1-6) and (A13-25). The sector-coupled system's constraints are delineated in equation (A1-25) along with the energy balance equations for each current configuration outlined in equation (A26-28).

Details on generating weather and demand scenarios are provided in the Supplementary materials. The IBM CPLEX solver is used to address the optimization challenge. The mathematical programming codes are publicly accessible via the GitHub link provided in the Data availability section.

Table 1. Economic parameters of facilities. (benchmarked in 2040)

Component	Lifetime (year)	Investment cost	O&M cost (% of installation cost)	Reference
Wind turbine	30	0.95 MM\$/MW	2.4%	[20, 45]
PV panel	35	0.6 MM\$/MW	2%	[20, 45]
Battery (8 h)	10	0.161 MM\$/MWh	2.5%	[20, 45]
PEM electrolyzer	10	0.44 MM\$/MW	2%	[20, 46]

Alkaline electrolyzer	10	0.33 MM\$/MW	2%	[20, 46]
Fuel cell	5	0.96 MM\$/MW	2%	[38]
Hydrogen tank	25	0.25 MM\$/t H ₂	1%	[20]
Solid DAC plant	30	2.76 MM\$/t CO ₂ • h	4%	[47]
Heat pump	25	0.0633 MM\$/MW	0.36%	[47]
Thermal energy storage	30	0.025 MM\$/MWh _{th}	0.02%	[14]

Data availability

The datasets generated and the original codes of mathematical programming are available from the public GitHub by the following link: <https://github.com/SunBooGermany/DAC-GH-System>. The detail parameters value and the description will be updated after the final acceptance or reasonable request from editors and reviewers.

Conflicts of interest

There are no conflicts of interest to declare

Acknowledgements

The authors acknowledge that this work was supported by the KAIST-Aramco CO₂ management center.

1. Liu, S., et al., *Direct air capture of CO₂ via cyclic viologen electrocatalysis*. Energy & Environmental Science, 2024. **17**(3): p. 1266-1278.
2. Sharifian, R., et al., *Electrochemical carbon dioxide capture to close the carbon cycle*. Energy & Environmental Science, 2021. **14**(2): p. 781-814.
3. Holmes, H.E., M.J. Realff, and R.P. Lively, *Water management and heat integration in direct air capture systems*. Nature Chemical Engineering, 2024. **1**(3): p. 208-215.
4. Jacobson, M.Z., *The health and climate impacts of carbon capture and direct air capture*. Energy & Environmental Science, 2019. **12**(12): p. 3567-3574.

5. Küng, L., et al., *A roadmap for achieving scalable, safe, and low-cost direct air carbon capture and storage*. Energy & Environmental Science, 2023. **16**(10): p. 4280-4304.
6. Breyer, C., et al., *Direct Air Capture of CO₂: A Key Technology for Ambitious Climate Change Mitigation*. Joule, 2019. **3**(9): p. 2053-2057.
7. Bui, M., et al., *Carbon capture and storage (CCS): the way forward*. Energy & Environmental Science, 2018. **11**(5): p. 1062-1176.
8. Bachman, E., et al., *Rail-based direct air carbon capture*. Joule, 2022. **6**(7): p. 1368-1381.
9. Young, J., et al., *The impact of binary water–CO₂ isotherm models on the optimal performance of sorbent-based direct air capture processes*. Energy & Environmental Science, 2021. **14**(10): p. 5377-5394.
10. Sabatino, F., et al., *A comparative energy and costs assessment and optimization for direct air capture technologies*. Joule, 2021. **5**(8): p. 2047-2076.
11. Breyer, C., M. Fasihi, and A. Aghahosseini, *Carbon dioxide direct air capture for effective climate change mitigation based on renewable electricity: a new type of energy system sector coupling*. Mitigation and Adaptation Strategies for Global Change, 2019. **25**(1): p. 43-65.
12. Young, J., et al., *Process-informed adsorbent design guidelines for direct air capture*. Chemical Engineering Journal, 2023. **456**.
13. Erans, M., et al., *Direct air capture: process technology, techno-economic and socio-political challenges*. Energy & Environmental Science, 2022. **15**(4): p. 1360-1405.
14. Yang, L. and X. Wu, *Net-zero carbon configuration approach for direct air carbon capture based integrated energy system considering dynamic characteristics of CO₂ adsorption and desorption*. Applied Energy, 2024. **358**.
15. Shirizadeh, B., et al., *Towards a resilient and cost-competitive clean hydrogen economy: the future is green*. Energy & Environmental Science, 2023. **16**(12): p. 6094-6109.
16. Liu, H., et al., *Pathway toward cost-effective green hydrogen production by solid oxide electrolyzer*. Energy & Environmental Science, 2023. **16**(5): p. 2090-2111.
17. Staffell, I., et al., *The role of hydrogen and fuel cells in the global energy system*. Energy & Environmental Science, 2019. **12**(2): p. 463-491.
18. Park, J., et al., *Techno-economic analysis of solar powered green hydrogen system based on multi-objective optimization of economics and productivity*. Energy Conversion and Management, 2024. **299**.
19. Won, W., et al., *Design and operation of renewable energy sources based hydrogen supply system: Technology integration and optimization*. Renewable Energy, 2017. **103**: p. 226-238.
20. Terlouw, T., et al., *Large-scale hydrogen production via water electrolysis: a techno-economic and environmental assessment*. Energy & Environmental Science, 2022. **15**(9): p. 3583-3602.
21. Voronova, A., et al., *Systematic degradation analysis in renewable energy-powered proton exchange membrane water electrolysis*. Energy & Environmental Science, 2023. **16**(11): p. 5170-5184.
22. Hu, K., et al., *Comparative study of alkaline water electrolysis, proton exchange membrane water electrolysis and solid oxide electrolysis through multiphysics modeling*. Applied Energy, 2022. **312**.
23. Park, J., et al., *Green hydrogen to tackle the power curtailment: Meteorological data-based capacity factor and techno-economic analysis*. Applied Energy, 2023. **340**.

24. Joos, M. and I. Staffell, *Short-term integration costs of variable renewable energy: Wind curtailment and balancing in Britain and Germany*. Renewable and Sustainable Energy Reviews, 2018. **86**: p. 45-65.
25. Ramsebner, J., et al., *The sector coupling concept: A critical review*. WIREs Energy and Environment, 2021. **10**(4).
26. Bernath, C., G. Deac, and F. Sensfuß, *Impact of sector coupling on the market value of renewable energies – A model-based scenario analysis*. Applied Energy, 2021. **281**.
27. Gea-Bermúdez, J., et al., *The role of sector coupling in the green transition: A least-cost energy system development in Northern-central Europe towards 2050*. Applied Energy, 2021. **289**.
28. Castro-Amoedo, R., et al., *On the role of system integration of carbon capture and mineralization in achieving net-negative emissions in industrial sectors*. Energy & Environmental Science, 2023. **16**(10): p. 4356-4372.
29. Brown, T., et al., *Synergies of sector coupling and transmission reinforcement in a cost-optimised, highly renewable European energy system*. Energy, 2018. **160**: p. 720-739.
30. He, G., et al., *Sector coupling via hydrogen to lower the cost of energy system decarbonization*. Energy & Environmental Science, 2021. **14**(9): p. 4635-4646.
31. Chauhan, A. and R.P. Saini, *A review on Integrated Renewable Energy System based power generation for stand-alone applications: Configurations, storage options, sizing methodologies and control*. Renewable and Sustainable Energy Reviews, 2014. **38**: p. 99-120.
32. Bukar, A.L., et al., *A rule-based energy management scheme for long-term optimal capacity planning of grid-independent microgrid optimized by multi-objective grasshopper optimization algorithm*. Energy Convers Manag, 2020. **221**: p. 113161.
33. Bukar, A.L., C.W. Tan, and K.Y. Lau, *Optimal sizing of an autonomous photovoltaic/wind/battery/diesel generator microgrid using grasshopper optimization algorithm*. Solar Energy, 2019. **188**: p. 685-696.
34. Liu, T., et al., *Techno-economic feasibility of solar power plants considering PV/CSP with electrical/thermal energy storage system*. Energy Conversion and Management, 2022. **255**.
35. Andersson, J. and S. Grönkvist, *Large-scale storage of hydrogen*. International Journal of Hydrogen Energy, 2019. **44**(23): p. 11901-11919.
36. Buttler, A. and H. Spliethoff, *Current status of water electrolysis for energy storage, grid balancing and sector coupling via power-to-gas and power-to-liquids: A review*. Renewable and Sustainable Energy Reviews, 2018. **82**: p. 2440-2454.
37. Grigoriev, S.A., et al., *Current status, research trends, and challenges in water electrolysis science and technology*. International Journal of Hydrogen Energy, 2020. **45**(49): p. 26036-26058.
38. Nayak-Luke, R.M. and R. Bañares-Alcántara, *Techno-economic viability of islanded green ammonia as a carbon-free energy vector and as a substitute for conventional production*. Energy & Environmental Science, 2020. **13**(9): p. 2957-2966.
39. Wiegner, J.F., et al., *Optimal Design and Operation of Solid Sorbent Direct Air Capture Processes at Varying Ambient Conditions*. Industrial & Engineering Chemistry Research, 2022. **61**(34): p. 12649-12667.
40. Kim, S., et al., *Multi-period, multi-timescale stochastic optimization model for simultaneous capacity investment and energy management decisions for hybrid Micro-Grids with green hydrogen production under uncertainty*. Renewable and Sustainable Energy Reviews, 2024. **190**.

41. Niblett, D., et al., *Review of next generation hydrogen production from offshore wind using water electrolysis*. Journal of Power Sources, 2024. **592**.
42. Meesenburg, W., et al., *Optimizing control of two-stage ammonia heat pump for fast regulation of power uptake*. Applied Energy, 2020. **271**.
43. You, F., J.M. Wassick, and I.E. Grossmann, *Risk management for a global supply chain planning under uncertainty: Models and algorithms*. AIChE Journal, 2009. **55**(4): p. 931-946.
44. Yeh, K., et al., *Two stage stochastic bilevel programming model of a pre-established timberlands supply chain with biorefinery investment interests*. Computers & Chemical Engineering, 2015. **73**: p. 141-153.
45. Vimmerstedt, L., et al., *Annual Technology Baseline: The 2022 Electricity Update*. 2022, National Renewable Energy Lab.(NREL), Golden, CO (United States).
46. Böhm, H., et al., *Projecting cost development for future large-scale power-to-gas implementations by scaling effects*. Applied Energy, 2020. **264**.
47. Fasihi, M., O. Efimova, and C. Breyer, *Techno-economic assessment of CO2 direct air capture plants*. Journal of Cleaner Production, 2019. **224**: p. 957-980.

Integrating solid direct air capture systems with green hydrogen production: Economic synergy of sector coupling

Supporting information

Sunwoo Kim^{1,2}, Joungho Park³, and Jay H. Lee^{1*}

¹ Mork Family Department of Chemical Engineering and Material Sciences, University of Southern California, 925 Bloom Walk, Los Angeles, CA 90089, USA

² Department of Chemical and Biomolecular Engineering, Korea Advanced Institute of Science and Technology (KAIST), 291, Daehak-ro, Yuseong-gu, Daejeon, 34141, Republic of Korea

³ Energy AI & Computational Science Laboratory, Korea Institute of Energy Research, 71-2 Jang-dong, Yuseong-gu, Daejeon, 305-343, Republic of Korea

* Corresponding author's E-mail: jlee4140@usc.edu

Table of contents

A. Models used.....	2
A. 1. Wind turbine	
A. 2. Solar PV panel	
A. 3. Battery	
A. 4. Water electrolyzer	
A. 5. Fuel cell	
A. 6. Gaseous hydrogen tank	
A. 7. Electrified heat pump	
A. 8. Thermal energy storage	
A. 9. Solid DAC plant	
B. Sector coupled system description of DC configuration and AC configuration.....	10
C. Weather and demand scenarios generation.....	12
D. Influence of number of weather scenario used in Two-stage stochastic programming	13
E. Influence of the duration of battery in the economic viability.....	14
F. Reference.....	15

A. Models used

A. 1. Wind turbine

The model for a 5-MW turbine from the National Renewable Energy Laboratory (NREL) is utilized, formulated as follows:[1]

$$P_{sc,t}^T = \begin{cases} \eta^C \times X_T \times (\alpha \times WS^{sc,t3} + \beta) & \text{for } WS^{ci} < WS^{sc,t} \leq WS^r \\ \eta^C \times X_T \times P^{rated} & \text{for } WS^r < WS^{sc,t} \leq WS^{co} \\ 0 & \text{for } WS^{sc,t} \leq WS^{ci} \text{ or } WS^{sc,t} > WS^{co} \end{cases} \quad (A1)$$

In this equation, $P_{sc,t}^T$ represents the power output from the turbine, η^C denotes the efficiency of the appropriate converter, and X_T represents the capacity of turbine. This model includes critical wind speed thresholds: the *cut-in* speed (WS^{ci}), *rated* speed (WS^r), and *cut-out* speed (WS^{co}). The parameters α and β describe the turbine's power output characteristics for wind speeds lying between the cut-in and cut-out thresholds. The power increases with wind speed until reaching the rated power rate (P^{rated}). The turbine ceases to generate power if the wind speed falls below the cut-in speed or surpasses the cut-out speed.

A. 2. Solar PV panel

The power generated from a solar photovoltaic (PV) panel is defined by the following equation:[2, 3]

$$P_{sc,t}^P = \eta^C \times X_P \times \left[1 + \gamma \times \left(T^{sc,t} + GHI^{sc,t} \times \frac{NOCT - 20}{800} - T^{ref} \right) \right] \times \frac{GHI^{sc,t}}{1000} \quad (A2)$$

In this equation, $P_{sc,t}^P$ represents the power generated from the PV panel, η^C denotes the efficiency of the appropriate converter, and X_P is the PV panel's capacity. γ (-0.0037 K^{-1}), is the temperature coefficient, affecting the panel's performance relative to the cell temperature ($T^{sc,t}$). $GHI^{sc,t}$ stands for the global horizontal solar irradiance (GHI) at a specific scenario and time, the normal operating cell temperature ($NOCT$) is set at $45 \text{ }^\circ\text{C}$, and T^{ref} (298.15 K) represents the reference ambient temperature.

A. 3. Battery

This study employs a 8-hour battery system, designed to complete a full charge and discharge cycle within a 8-hour timeframe, as detailed in eqn (A3) and (A4). The dynamics of energy storage within the battery ($ESS_{sc,t}$, unit: MWh) are governed by various factors such as the self-discharging rates (σ^B), the charging ($ch_{sc,t}$, unit: MW) and discharging ($dch_{sc,t}$, unit: MW) rates, and the overall battery efficiency (η^B), as elaborated in eqn (A5). The self-discharging rate is assumed to be 0.0083% per hour and the efficiency is assumed to be 95%. Furthermore, we stipulate that the battery's storage level should be maintained within 15% to 95% of its rated capacity, as expressed in eqn (A6).[4]

$$0 \leq ch_{sc,t} \leq 0.125 \times X_B \quad (\text{A3})$$

$$0 \leq dch_{sc,t} \leq 0.125 \times X_B \quad (\text{A4})$$

$$ESS_{sc,t} = (1 - \sigma^B) \times ESS_{sc,t-1} + \left(\eta^C \times \eta^B \times ch_{sc,t} - \frac{1}{\eta^C \times \eta^B} \times dch_{sc,t} \right) \times \Delta t \quad (\text{A5})$$

$$0.15 \times X_B \leq ESS_{sc,t} \leq 0.95 \times X_B \quad (\text{A6})$$

A. 4. Water electrolyzer

This study utilizes a proton exchange membrane (PEM) water electrolyzers and Alkaline electrolyzers to split water into hydrogen and oxygen gases. The PEM electrolyzers employ a solid polymer membrane to conduct protons from the anode to the cathode, effectively preventing the mixing of gases. In contrast, Alkaline electrolyzers employ an anion exchange membrane for gas separation. This distinction in membrane type fundamentally alters the electrolysis process, as alkaline electrolyzers utilize an aqueous alkaline solution as the electrolyte. By utilizing a liquid electrolyte, alkaline electrolyzers eliminate the need for the expensive and fragile proton exchange membrane, potentially offering cost advantages and improved durability compared to PEM electrolyzers. Despite of the high cost, PEM electrolyzers have notable benefits by high operational efficiency and swift response times to demand fluctuations. Furthermore, the PEM electrolyzer is distinguished by its ability to produce high-purity hydrogen gas and its capacity to operate efficiently at low minimum loads (min^W)—significantly lower than those required by alkaline electrolyzers (20%), with a typical minimum load of 5%. [5, 6]. The assumed energy efficiency (η^W) for the PEM electrolyzer is 48 kWh per kilogram of hydrogen, and 50 kWh per kilogram of hydrogen for alkaline electrolyzer. The unit of $p2h_{sc,t}$ and the unit of X_W is MW. The operational parameters and constraints of the PEM electrolyzer are detailed in the subsequent equation.

$$\min^W \times X_W \leq p2h_{sc,t} \leq X_W \quad (\text{A7})$$

A. 5. Fuel cell

This research utilizes a PEM fuel cell for the generation of electricity from hydrogen stored. Fuel cells are innovative devices that directly convert the chemical energy of a fuel into electrical energy, presenting clear advantages over conventional combustion technologies. A primary advantage of hydrogen fuel cells is their environmental friendliness; they emit only water as a byproduct, significantly contributing to the reduction of CO₂ emissions and other air

pollutants.[7] For the purposes of this study, the energy conversion efficiency (η^{FC}) of the PEM fuel cells is assumed to be 20.4 kWh per kilogram of hydrogen. The unit of both $h2p_{sc,t}$ and X_{FC} is MW. The operational parameters and constraints governing the use of the PEM fuel cell are outlined in the equation that follows.

$$0 \leq h2p_{sc,t} \leq X_{FC} \quad (A8)$$

A. 6. Gaseous hydrogen tank

This research utilizes a gaseous HT system, designed to store hydrogen under high pressure to efficiently accommodate large volumes of hydrogen gas.[8] The volume of hydrogen stored in the HT ($HT_{sc,t}$, unit: ton of hydrogen) is determined by various factors, including the self-leakage rate (σ^{HT}), the rate of hydrogen production from the electrolyzer, and the rate of hydrogen consumption by the fuel cell, as detailed in eqn (A9). For every week, there is a demand for hydrogen ($D_{sc,w}^H$) to be satisfied. Consequently, the balance equation for the HT is adjusted accordingly to reflect this demand, as shown in eqn (A10). The self-leakage rate of the HT is assumed to be 0.0104% per hour, accounting for the minimal loss of stored hydrogen over time due to imperfections in the tank's containment system. Additionally, it is crucial that the HT's storage level does not surpass its designed capacity to ensure safety and maintain the integrity of the storage system, as indicated in eqn (A11). This constraint is essential for preventing overpressure scenarios and ensuring the operational reliability of the hydrogen storage system

$$HT_{sc,t} = (1 - \sigma^{HT}) \times HT_{sc,t-1} + \left(\frac{\eta^C}{\eta^W} \times p2h_{sc,t} - \frac{1}{\eta^{FC}} \times h2p_{sc,t} \right) \times \Delta t \quad (A9)$$

$$HT_{sc,t} = (1 - \sigma^{HT}) \times HT_{sc,t-1} + \left(\frac{\eta^C}{\eta^W} \times p2h_{sc,t} - \frac{1}{\eta^{FC}} \times h2p_{sc,t} \right) \times \Delta t - D_{sc,w}^H \quad (A10)$$

$$0 \leq HT_{sc,t} \leq X_{HT} \quad (A11)$$

The energy balance equation for the GH system can be expressed as below:

$$P_{sc,t}^T + P_{sc,t}^P - ch_{sc,t} + dch_{sc,t} - out_{sc,t} + \eta^C \times h2p_{sc,t} - p2h_{sc,t} = 0 \quad (A12)$$

A. 7. Electrified heat pump

The electrified heat pump in this study is designed to convert electrical power into thermal energy, specifically generating superheated steam, by harnessing electricity. It operates with a minimum operating ratio ($p2t^{min}$) of its rated capacity (X_{HP} , unit: MW), which is a

critical parameter for ensuring efficient operation without underutilization of its potential, as elaborated in eqn (A13), where the unit of $p2t_{sc,t}$ is also MW. Initially, $p2t^{min}$ is set at 0.4 for the base case analysis, indicating that the heat pump must operate at least 40% of its rated capacity.[9] To explore the economic implications of varying operational efficiencies, further analysis includes scenarios where $p2t^{min}$ is reduced to 0.1, assessing the impact of increased flexibility on system economics.[10, 11] The heat pump's coefficient of performance (COP) is assumed to be 3.41, signifying that for every unit of electrical energy consumed, the heat pump produces 3.41 units of thermal energy.[12]

$$p2t^{min} \times X_{HP} \leq p2t_{sc,t} \leq X_{HP} \quad (A13)$$

A. 8. Thermal energy storage

This study incorporates the use of a superheated steam-based TES system, designed to operate at 40% of its rated capacity (X_{TES} , unit: MW_{th}) for both charging and discharging process, as expressed in eqn (A14) and (A15). The quantity of thermal energy stored in the TES ($TES_{sc,t}$, unit: MWh_{th}) is influenced by a variety of factors including the self-discharge rate (σ^{TES}), charging ($Tch_{sc,t}$, unit: MW_{th}) and discharging ($Tdch_{sc,t}$, unit: MW_{th}) rates, and the overall efficiency of the TES system (η^{TES}), as elaborated in eqn (A16). The self-discharge rate accounting for thermal energy losses over time even without active discharge, is set at 0.5% per hour, while the overall efficiency is assumed to be 98%, indicating a high level of energy conservation during storage operations.[10] Additionally, it is stipulated that the TES system's energy storage level is regulated to stay within 10% to 90% of its rated capacity, as expressed in eqn (A17). This range ensures optimal operation and longevity of the storage system by preventing conditions that could lead to underutilization or overstrain of the TES capabilities, thereby maintaining its effectiveness and reliability in energy storage and retrieval operations.

$$Tch_{sc,t} \leq 0.4 \times X_{TES} \quad (A14)$$

$$Tdch_{sc,t} \leq 0.4 \times X_{TES} \quad (A15)$$

$$TES_{sc,t} = (1 - \sigma^{TES}) \times TES_{sc,t-1} + \left(\eta^{TES} \times Tch_{sc,t} - \frac{1}{\eta^{TES}} \times Tdch_{sc,t} \right) \times \Delta t \quad (A16)$$

$$0.1 \times X_{TES} \leq TES_{sc,t} \leq 0.9 \times X_{TES} \quad (A17)$$

A. 9. Solid DAC plant

This study employs a solid DAC plant, comprising numerous modularized units, each with a rated capacity of 50 t CO₂ per year.[13] These modularized units are designed to operate independently, allowing for flexibility in their operation. There is a distinct sequential constraint between the two operational phases of the DAC process, as well as the possibility of shutdowns, as illustrated in below figure:

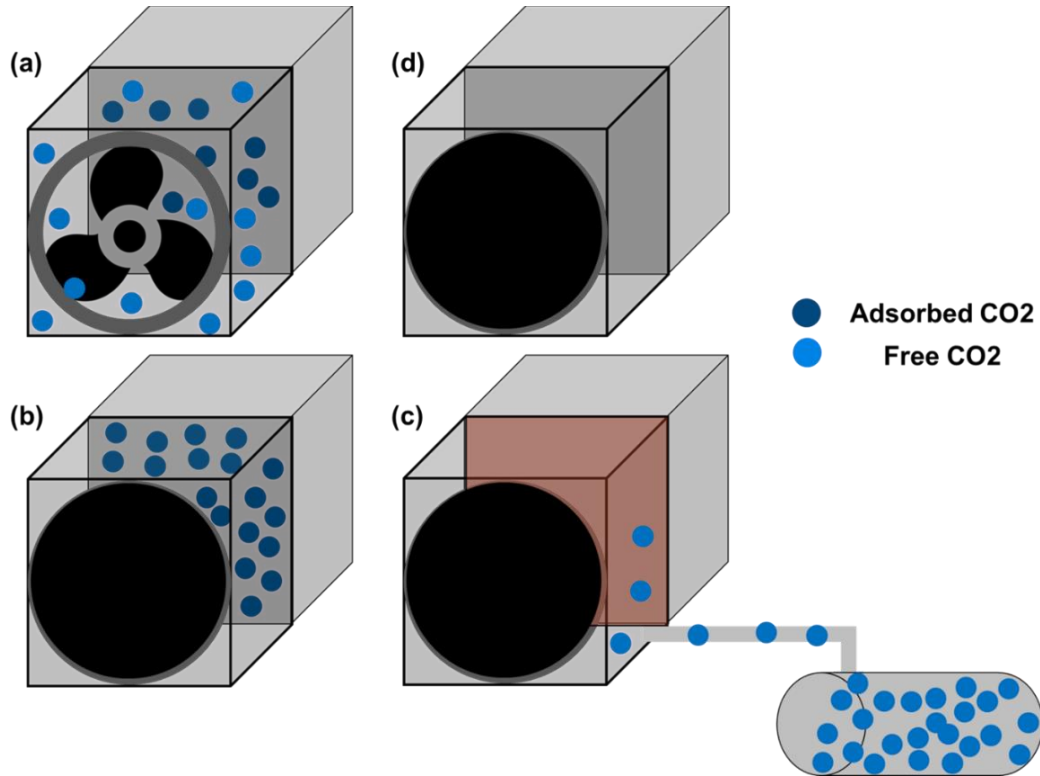


Fig. A. 1. Sequential batch process of the solid DAC system, detailing the operational phases and shutdown periods. In the figure, (a) indicates the adsorption phase where CO₂ is captured from the atmosphere, (b) represents a shutdown period following the adsorption phase, allowing for any necessary system adjustments or maintenance, (c) denotes the desorption phase during which the captured CO₂ is released from the adsorbent material for storage or use, and (d) represents a shutdown period after desorption, preparing the system for the next adsorption cycle. This sequence ensures the efficient capture and release of CO₂ in a cyclic manner.

Fig. A. 1 illustrates the operational phases of the solid DAC system, focusing on the dynamics of CO₂ capture and the associated energy consumption. Fig. A. 1 (a) showcases the adsorption phase, where ventilation is activated to increase air flow over the adsorbent, enhancing CO₂ capture given its low atmospheric concentration.[10] During this phase, CO₂ is adsorbed to the solid adsorbent and the remaining air is expelled, which requires electrical energy for the ventilation system. Fig. A. 1 (b) details the post-adsorption shutdown. After adsorption, closing the air passages of the modular unit traps CO₂ within. This stage does not consume energy, presenting an opportunity for operational pause when renewable energy

supply is low, retaining the captured CO₂ for subsequent desorption. Fig. A. 1 (c) describes the desorption phase, where the adsorbent is heated to approximately 100 °C to release the captured CO₂. [11] A vacuum pump is employed to aid in CO₂ collection, marking this phase as the most energy-intensive, consuming both electrical and thermal energy. Fig. A. 1 (d) covers the post-desorption shutdown, an energy-free phase allowing for operational breaks following CO₂ release, preparing the system for the next adsorption cycle.

The sequential operational relationship between these phases is further elaborated in Fig. A. 2 and defined through eqn (A18-23). A unit in state (a) can progress to state (b) or (c); from state (b), it can remain or move to state (c); in state (c), it can shift to state (d) or revert to state (a); and from state (d), it can either stay or transition back to state (a). This cyclical and strategic progression between states underscores the system's operational flexibility and energy management in solid DAC processes.

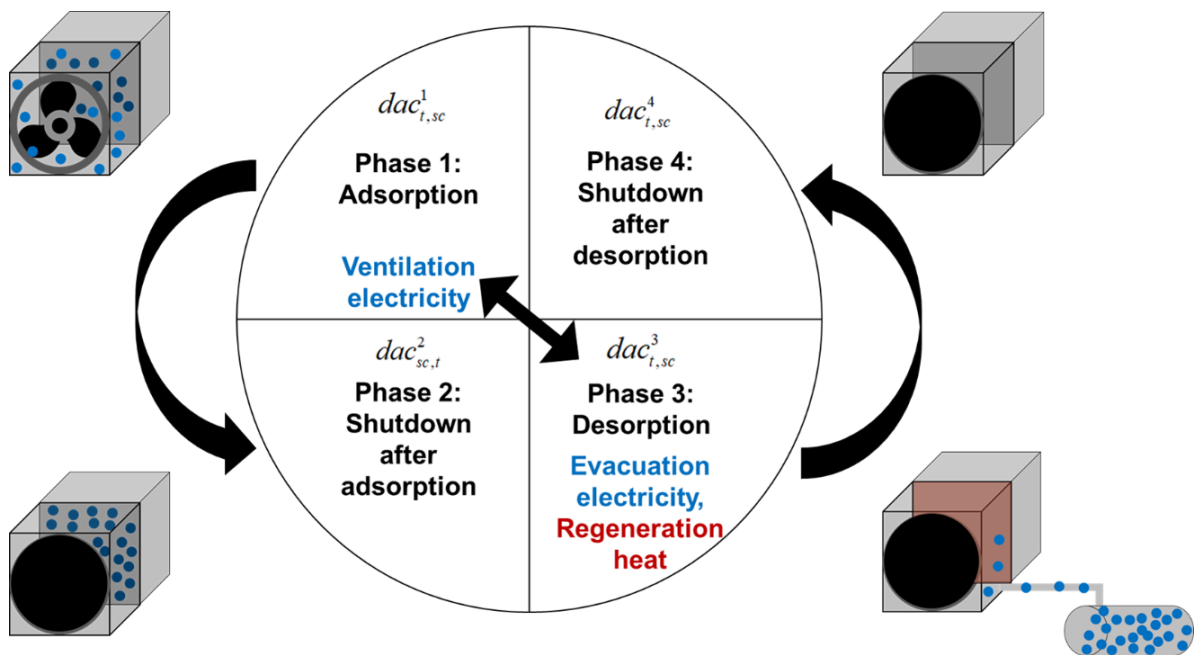


Fig. A. 2. Description of variables and their interrelations across the various phases of solid DAC system, highlighting the energy consumption characteristics of each phase.

$$0 \leq dac_{sc,t}^1, dac_{sc,t}^2, dac_{sc,t}^3, dac_{sc,t}^4 \leq 2 \times X_{DAC} \quad (A18)$$

$$dac_{sc,t}^1 + dac_{sc,t}^2 + dac_{sc,t}^3 + dac_{sc,t}^4 = 2 \times X_{DAC} \quad (A19)$$

$$dac_{t+1,sc}^1 \leq dac_{t,sc}^3 + dac_{t,sc}^4 \quad (A20)$$

$$dac_{t+1,sc}^3 \leq dac_{t,sc}^1 + dac_{t,sc}^2 \quad (A21)$$

$$dac_{t+1,sc}^2 = dac_{t,sc}^2 + dac_{t,sc}^1 - dac_{t+1,sc}^3 \quad (A22)$$

$$dac_{t+1,sc}^4 = dac_{t,sc}^4 + dac_{t,sc}^3 - dac_{t+1,sc}^1 \quad (A23)$$

In above equations, $dac_{sc,t}^k$ (unit: t CO₂/hr) denotes the capable CO₂ flow rate of DAC plant at phase k , and X_{DAC} (unit: t CO₂/hr) represents the capability of DAC plant, reducing CO₂ through the entire process encompassing the adsorption and the desorption. Here, the multiplication by 2 accounts for the complete cycle time.

In this analysis, given our focus on achieving CO₂ reduction targets ranging from 0.1 Mt to 1.3 Mt per year, the total count of modular units required falls within the thousands to tens of thousands range. Consequently, while the variable representing the quantity of solid DAC system units is inherently discrete, for the purposes of this study, it is treated as a continuous variable to simplify calculations and modeling. Furthermore, it is assumed that all units operate with uniform energy efficiency and cycle times, with both the adsorption and desorption phases lasting 1 hour each.

For the adsorption phase, the energy consumption is estimated at 0.07 MWh per ton of CO₂ captured (e^1). During the desorption phase, the energy requirements are assumed to be 0.14 MWh of electrical energy (e^3) and 1.286 MWh of thermal energy (h^3) per ton of CO₂. [12] These assumptions allow for a simplified yet realistic approximation of the energy inputs necessary for the operation of the solid DAC system. The thermal and electricity energy balance equations for the solid DAC system can be expressed in eqn (A24) and eqn (A25), respectively.

$$\eta^C \times COP \times p2t_{sc,t} - h^3 \times dac_{sc,t}^3 - Tch_{sc,t} + Tdch_{sc,t} = 0 \quad (A24)$$

$$P_{sc,t}^T + P_{sc,t}^P - ch_{sc,t} + dch_{sc,t} - out_{sc,t} - e^1 \times dac_{sc,t}^1 - e^3 \times dac_{sc,t}^3 - p2t_{sc,t} = 0 \quad (A25)$$

Energy balance equations for the combined system vary according to the specific current configuration and are summarized below:

DC or AC configuration:

$$P_{sc,t}^T + P_{sc,t}^P - ch_{sc,t} + dch_{sc,t} - out_{sc,t} + \eta^C \times h2p_{sc,t} - p2h_{sc,t} - e^1 \times dac_{sc,t}^1 - e^3 \times dac_{sc,t}^3 - p2t_{sc,t} = 0 \quad (A26)$$

AC-DC configuration:

$$P_{sc,t}^P - ch_{sc,t} + dch_{sc,t} + \eta^C \times h2p_{sc,t} - p2h_{sc,t} - D2A_{sc,t} + \eta^C \times A2D_{sc,t} = 0 \quad (A27)$$

$$P_{sc,t}^T - ch_{sc,t}^2 + dch_{sc,t}^2 - out_{sc,t} + \eta^C \times D2A_{sc,t} - A2D_{sc,t} - e^1 \times dac_{sc,t}^1 - e^3 \times dac_{sc,t}^3 - p2t_{sc,t} = 0 \quad (A28)$$

B. Sector coupled system description of DC configuration and AC configuration.

The diagrams illustrate the sector coupled system of DC configuration and AC configuration are presented here. Among the current conversion configurations analyzed, the DC to AC setup is identified as the most efficient for the integrated system, as demonstrated in Fig. B. 1-2. The economic advantages stemming from this sector-coupling depend significantly on the current configuration as illustrated in Fig. B. 3. The AC-DC hybrid current configuration superior the other two current configurations for all regions and CO₂ removal rate in both electrolyzers.

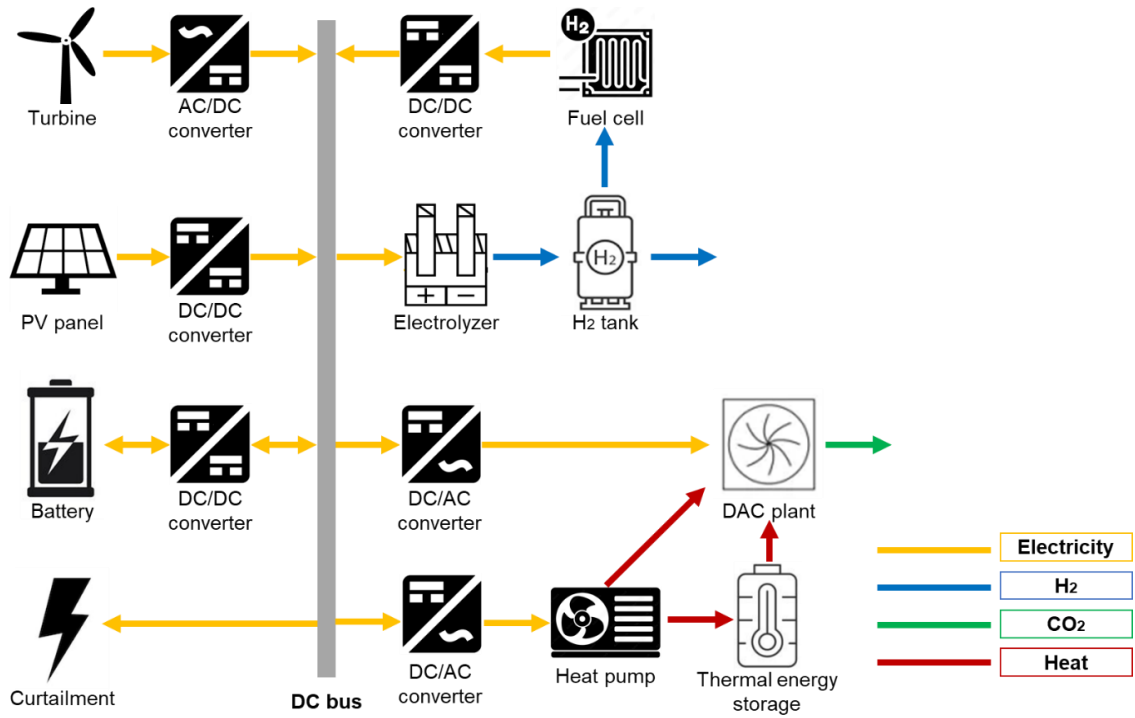


Fig. B. 1. Sector coupled system that merges Green Hydrogen (GH) production and solid Direct Air Capture (DAC), operating entirely in a Direct Current (DC) configuration. This system is engineered to meet hydrogen demand promptly and achieve a specified annual CO₂ reduction goal throughout the entirety of the project.

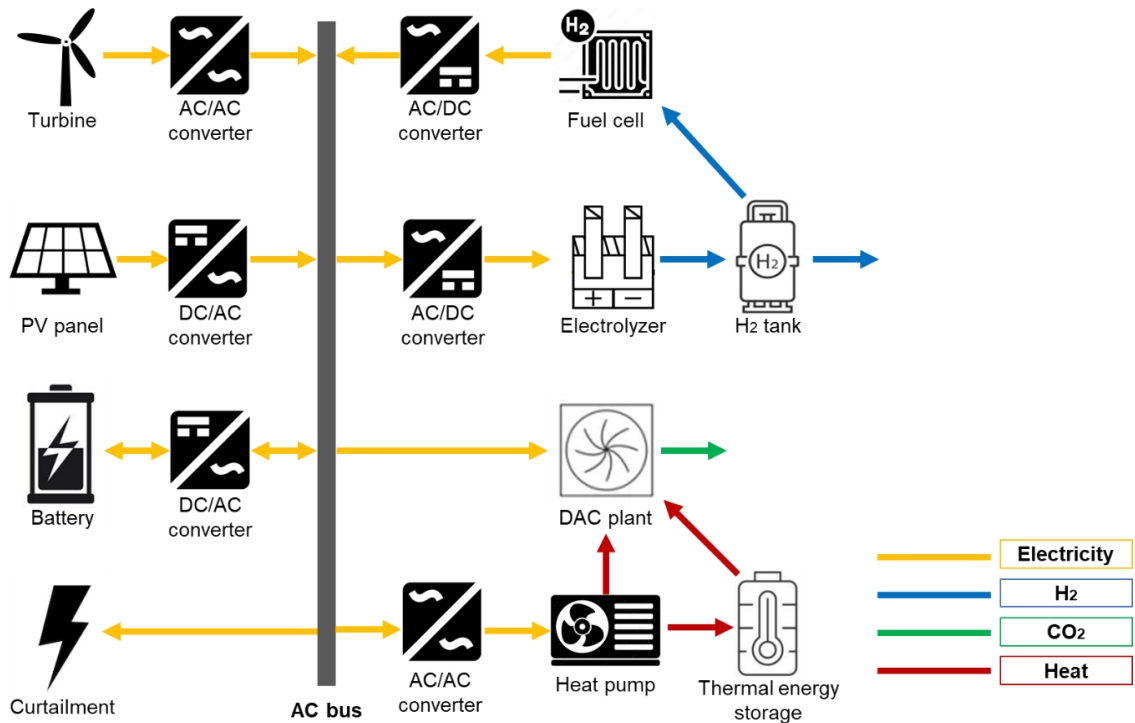


Fig. B. 2. Sector coupled system combining Green Hydrogen (GH) production with solid Direct Air Capture (DAC), functioning in an Alternating Current (AC) configuration. This arrangement aims to ensure the prompt fulfillment of hydrogen demand while also meeting

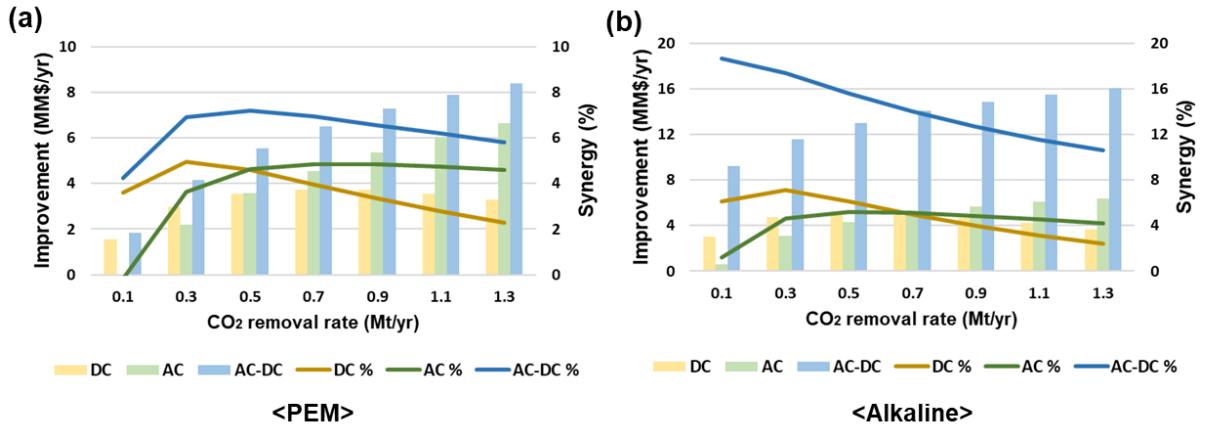


Fig. B. 3. Improvement (MM\$/yr) and Synergy (%) of sector coupling for each current configuration across different regions by varying CO₂ removal rate: (a) PEM electrolyzer-based sector coupled system, (b) Alkaline electrolyzer-based sector coupled system.

C. Weather and demand scenarios generation.

In this study, we conducted an extensive analysis in three regions to evaluate the improvement and characteristics of the proposed sector coupled system. We utilized hourly solar GHI data and wind speed data at observatory height obtained from National Solar Radiation Database (NSRDB) as summarized in Table C. 1.[14] The wind speed at 100 meters above the ground was compensated by using the Wind Atlas[15] to standardize these measurements for comparison. The wind speeds were adjusted to a reference height using the formula below:[16]

$$ws^{sc,t} = ws_{observatory}^{sc,t} \times \ln \frac{h}{z^{roughness}} \div \ln \frac{h^{observatory}}{z^{roughness}} \quad (C1)$$

In above equation, $ws_{observatory}^{sc,t}$ is the wind speed at the observatory, h is the hub height, $h^{observatory}$ indicates the observatory height, and $z^{roughness}$ denotes the roughness factor.

Table. C. 1. Summary of selected years and locations of the solar GHI and wind speed data.[17]

	Latitude	Longitude	Year
Antofagasta	-23.42	-70.49	2019–2021
Bundaberg	-24.87	152.45	2018–2020
Neom	27.97	35.50	2017–2019

*The spatial resolution is 2km by 2km and the temporal resolution is hourly.

D. Influence of number of weather scenario used in Two-stage stochastic programming

The current state of the art regarding the integration of weather data into the economic evaluation and design process of renewable energy systems lacks uniformity, primarily due to regional disparities and the specific objectives of the system in question. The incorporation of extensive seasonal data offers the advantage of fostering resilience and accuracy in system design and economic assessment. However, this approach amplifies the complexity of the optimization task exponentially, thus necessitating a careful balance.

In our recent session, we undertook an empirical study utilizing three annual weather data to assess economic viability. We juxtaposed the economic outcomes derived from one-year and two-year data averages against the comprehensive three-year dataset. Notably, employing a solitary year's data yielded discrepancies ranging from 2% to 6%, indicating inadequacy, whereas leveraging two years' data demonstrated an error margin within 1%. Consequently, we opted for the utilization of the complete three-year seasonal dataset to ensure robustness and accuracy in our economic evaluations.

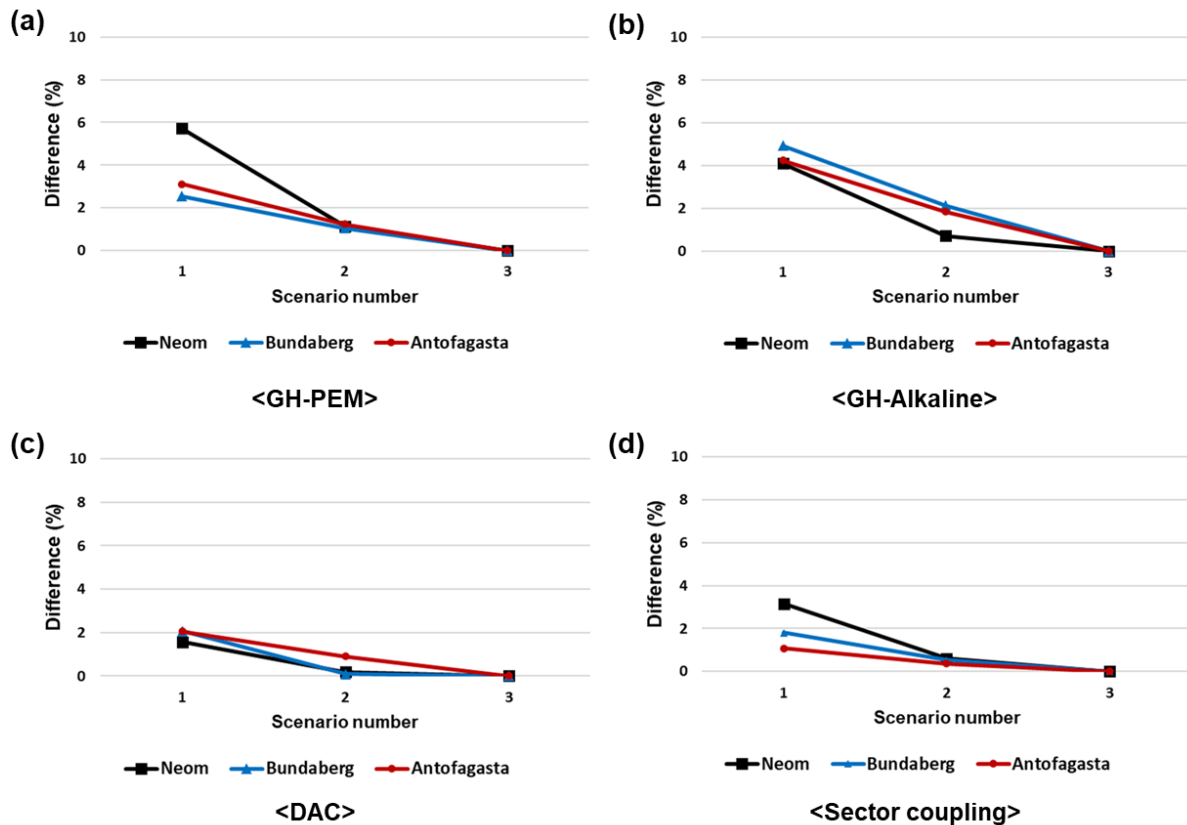


Fig. D. 1. Difference (%) variation by used annual scenario number: (a) PEM electrolyzer-based standalone green hydrogen system, (b) Alkaline electrolyzer-based standalone green hydrogen system, (c) Standalone DAC system, (d) Sector coupled system.

E. Influence of the duration of battery in the economic viability

We assess the economic viability of each system by varying the duration of battery usage. As elaborated in the preceding section, the duration of battery storage varies based on the energy capacity of the battery stack and the power rate capabilities of the system. Longer durations correlate with reduced power rate capabilities and lower unit costs per megawatt-hour (MWh), indicating a trade-off. A summary of the economic parameters is presented in Table E. 1.

We evaluate the economic feasibility of different battery durations and compute the TAC ratio relative to the economic value derived from utilizing a 4-hour battery for each system. As depicted in Fig. E. 1, the PEM electrolyzer-based standalone GH system favors a 6-hour battery duration, although the discrepancy among durations is minimal. Conversely, the alkaline electrolyzer exhibits significant variance among battery durations, with the 6-hour option offering the lowest cost. For both the standalone DAC system and the sector-coupled system, an 8-hour battery duration yields the lowest cost.

Table E. 1. Economic parameter for each duration of battery (benchmarked in 2040).

Battery (4 h)	10	0.19 MM\$/MWh	2.5%	[18, 19]
Battery (6 h)	10	0.171 MM\$/MWh	2.5%	[18, 19]
Battery (8 h)	10	0.161 MM\$/MWh	2.5%	[18, 19]
Battery (10 h)	10	0.155 MM\$/MWh	2.5%	[18, 19]

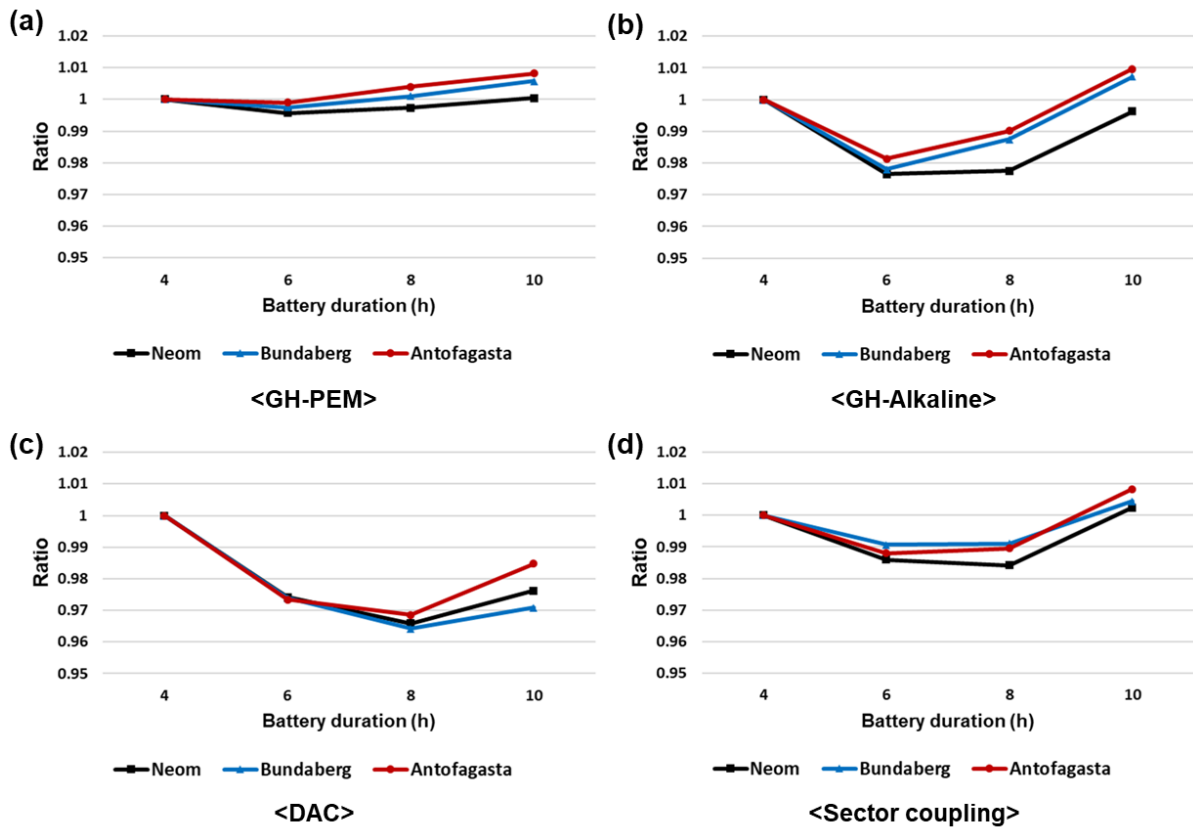


Fig. E. 1. TAC ratio of each system across different regions by varying duration of battery: (a) PEM electrolyzer-based standalone GH system, (b) Alkaline electrolyzer-based standalone GH system, (c) Standalone DAC system, (d) Sector coupled system.

F. Reference.

1. Chauhan, A. and R.P. Saini, *A review on Integrated Renewable Energy System based power generation for stand-alone applications: Configurations, storage options, sizing methodologies and control*. Renewable and Sustainable Energy Reviews, 2014. **38**: p. 99-120.
2. Bukar, A.L., et al., *A rule-based energy management scheme for long-term optimal capacity planning of grid-independent microgrid optimized by multi-objective grasshopper optimization algorithm*. Energy Convers Manag, 2020. **221**: p. 113161.
3. Bukar, A.L., C.W. Tan, and K.Y. Lau, *Optimal sizing of an autonomous photovoltaic/wind/battery/diesel generator microgrid using grasshopper optimization algorithm*. Solar Energy, 2019. **188**: p. 685-696.
4. Liu, T., et al., *Techno-economic feasibility of solar power plants considering PV/CSP with electrical/thermal energy storage system*. Energy Conversion and Management, 2022. **255**.
5. Buttler, A. and H. Spliethoff, *Current status of water electrolysis for energy storage, grid balancing and sector coupling via power-to-gas and power-to-liquids: A review*. Renewable and Sustainable Energy Reviews, 2018. **82**: p. 2440-2454.

6. Grigoriev, S.A., et al., *Current status, research trends, and challenges in water electrolysis science and technology*. International Journal of Hydrogen Energy, 2020. **45**(49): p. 26036-26058.
7. Nayak-Luke, R.M. and R. Bañares-Alcántara, *Techno-economic viability of islanded green ammonia as a carbon-free energy vector and as a substitute for conventional production*. Energy & Environmental Science, 2020. **13**(9): p. 2957-2966.
8. Andersson, J. and S. Grönkvist, *Large-scale storage of hydrogen*. International Journal of Hydrogen Energy, 2019. **44**(23): p. 11901-11919.
9. Meesenburg, W., et al., *Optimizing control of two-stage ammonia heat pump for fast regulation of power uptake*. Applied Energy, 2020. **271**.
10. Yang, L. and X. Wu, *Net-zero carbon configuration approach for direct air carbon capture based integrated energy system considering dynamic characteristics of CO₂ adsorption and desorption*. Applied Energy, 2024. **358**.
11. Wiegner, J.F., et al., *Optimal Design and Operation of Solid Sorbent Direct Air Capture Processes at Varying Ambient Conditions*. Industrial & Engineering Chemistry Research, 2022. **61**(34): p. 12649-12667.
12. Fasihi, M., O. Efimova, and C. Breyer, *Techno-economic assessment of CO₂ direct air capture plants*. Journal of Cleaner Production, 2019. **224**: p. 957-980.
13. McQueen, N., et al., *A review of direct air capture (DAC): scaling up commercial technologies and innovating for the future*. Progress in Energy, 2021. **3**(3).
14. Sengupta, M., et al., *The National Solar Radiation Data Base (NSRDB)*. Renewable and Sustainable Energy Reviews, 2018. **89**: p. 51-60.
15. Davis, N.N., et al., *The Global Wind Atlas: A high-resolution dataset of climatologies and associated web-based application*. Bulletin of the American Meteorological Society, 2023.
16. Wever, N., *Quantifying trends in surface roughness and the effect on surface wind speed observations*. Journal of Geophysical Research: Atmospheres, 2012. **117**(D11).
17. Kim, S., et al., *Techno-economic analysis for design and management of international green hydrogen supply chain under uncertainty: An integrated temporal planning approach*. Energy Conversion and Management, 2024. **301**.
18. Terlouw, T., et al., *Large-scale hydrogen production via water electrolysis: a techno-economic and environmental assessment*. Energy & Environmental Science, 2022. **15**(9): p. 3583-3602.
19. Vimmerstedt, L., et al., *Annual Technology Baseline: The 2022 Electricity Update*. 2022, National Renewable Energy Lab.(NREL), Golden, CO (United States).